ENVIRONMENTAL STUDIES

Uncontrolled deforestation and population growth threaten a tropical island's water and land resources in only 10 years

Anthony Foucher[1]*, Olivier Evrard[1], Laura Rabiet[1], Olivier Cerdan[2], Valentin Landemaine[2], Rémi Bizeul[1], Thomas Chalaux-Clergue[1], Jonathan Marescaux[3], Nicolas Debortoli[4], Valentin Ambroise[3], Jean-François Desprats[5]

Rapid demographic growth in tropical islands can exacerbate conflicts and pressures on natural resources, as illustrated by the French island of Mayotte where resources are limited. In only 10 years, uncontrolled migration and population growth (+80% of population between 2002 and 2021) have led to a pronounced 3600% increase in deforestation rates (2010–2014) and an intensification of agricultural practices, escalating conflicts over limited land, water, and biodiversity resources. Implementing an original multi-proxy approach to sediment cores, our study reveals a staggering 300% acceleration in erosion during the first wave of migration (2011–2015), followed by a further 190% increase (2019–2021) under sustained migratory and demographic pressures. Sedimentary DNA analysis provided insights into increased connectivity and community changes. By 2050, the population of this region will increase by 74 and 103%, in Comoros and Madagascar islands, respectively. Urgent conservation measures are needed to avoid major socio-environmental crises and to protect resources for future generations.

INTRODUCTION

Overpopulation and degradation of natural resources are intricately linked. According to the United Nations, the world population will reach 10.4 billion inhabitants by 2080 (*1*). Recent projections indicate that more than half of the global population change between 2020 and 2050 will take place in tropical regions of southeastern Asia and sub-Saharan Africa.

To respond to the global and local food demand associated with the massive population growth and the associated human migrations [e.g. for geopolitical, technologic, environmental, and climatic reasons (*2*, *3*)], agricultural intensification and cropland expansion are expected to occur in these tropical regions to boost agricultural production (*4*, *5*). These land use changes will affect the main biodiversity hotspots on Earth (*4*, *6*) and will represent the main driver of soil (e.g., soil infertility) and water degradation (e.g., decreasing of water storage capacity, contamination). They will also lead to an inexorable decline of biodiversity (*7*). These detrimental effects on soil, water, and biodiversity will be exacerbated in island contexts where natural resources are limited and human-environment interactions amplified across limited surface areas.

Mayotte Island (France, Comoros Archipelago) is one of these regions already endangered by overpopulation and land use changes (Fig. 1). This tropical island of 374 km^2 is affected since the beginning of the 2000s by a rapid and continuous population growth [+80% between 2002 and 2021 (310,000 inhabitants), considering only the official population] induced by an uncontrolled migration flow from neighboring islands (e.g., Comoros Islands, Madagascar). These migration dynamics are explained by geopolitical reasons, as this island changed status from an "oversea collectivity" ("*collectivité d'outre-mer*") to a proper "oversea department" ("*département d'outre-mer*") in 2011, and, as a result, it also became an outermost region of the European Union in 2014. This status change and the gradual transition to the same legal and social protection regime as in mainland France has led to an increase in illegal immigration. The resulting overpopulation (defined in this study as the situation where the current population exceeds the capacity that may be reasonably supported by the environment) of the island leads to a decline in the use of traditional and sustainable agricultural practices (a type of agroforestry referred to as Mayotte garden or "*jardin mahorais*") in favor of intensive monocultures (e.g., banana and cassava) aimed at increasing food production (*8*). The forest cover, which had increased notably between 1970 and 2000, has recently declined under the joint pressure of agricultural expansion and uncontrolled urbanization (Figs. 1 and 2). These changes induced an acceleration of soil erosion (e.g., landslides and muddy floods) and an excessive transfer of sediment and associated pollutants, contributing to the siltation of reservoirs providing the drinking water of the island (i.e., Dzoumogné and Combani reservoir (Figs. 1 and 2). This rapid agricultural expansion threatens biodiversity, soil resources, water quality and storage availability. The island has suffered since 2016 from several water crises as a combined result of overpopulation, the increase in drinking water needs per person, a higher need for irrigation, the more frequent occurrence of droughts, and the siltation of reservoirs with sediment limiting their storage capacity (Fig. 3). The transfer of sediment to the largest barrier reef–lagoon complex (1500 km^2) within the southwestern Indian Ocean (*9*) accelerates the siltation of the sea bed, threatening the marine fauna and flora, including the corals (*10*). The catchment of the Dzoumogné reservoir (1038 ha) (Figs. 1 and 2), located in the northern part of the island and where this current study took place, is facing all the abovementioned challenges. In 2003, this catchment was still largely covered by natural vegetation (62%) and managed with traditional practices (20%). In contrast, agricultural pressure led in 2022 to a decline of the forest and shrub formations (55%) and

[1]Laboratoire des Sciences du Climat et de l'Environnement (LSCE-IPSL), UMR 8212 (CEA-CNRS-UVSQ), Université Paris-Saclay, 91191 Gif-sur-Yvette Cedex, France. [2]BRGM, F-45060 Orléans, France. [3]E-BIOM, Rue Camille Hubert 11, Les Isnes, Belgium. [4]Namur Molecular Tech, CHU UCL, Namur, Belgium. [5]BRGM, F-34000 Montpellier, France.
*Corresponding author. Email: anthony.foucher@lsce.ipsl.fr

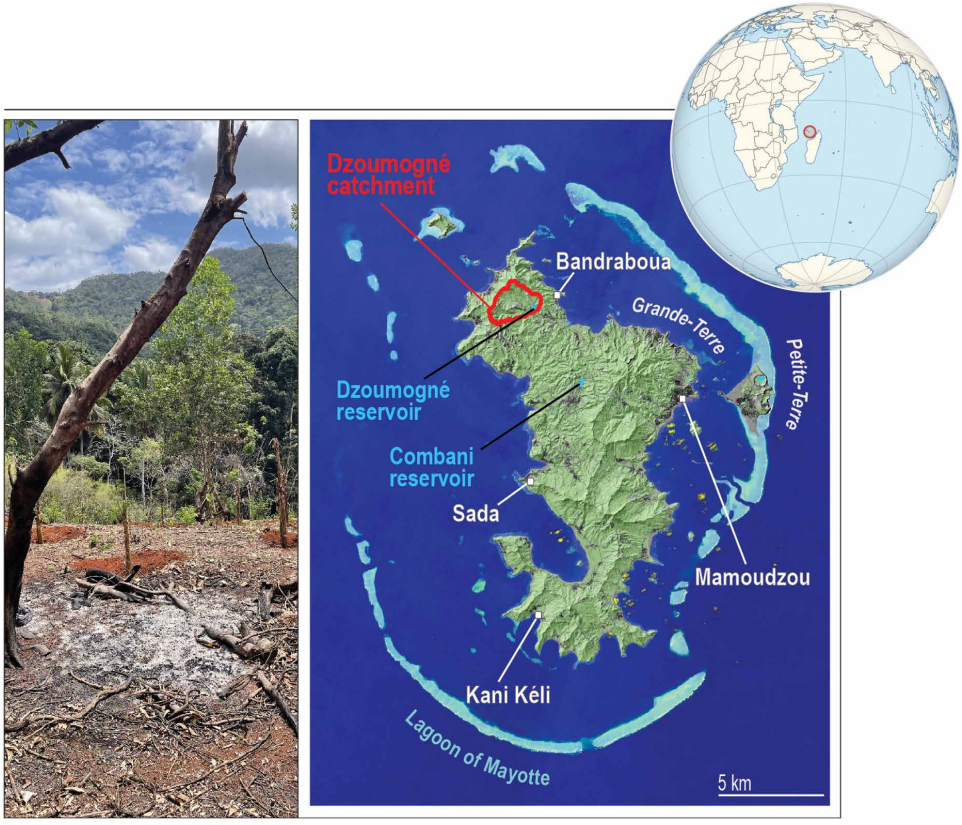

Fig. 1. Location of the Dzoumogné catchment within Mayotte Island. Mayotte Island, Comoros archipelago, France (**Right**), (sources: Landsat 7 ETM+ collection 1 2020-09-07 and IGN BD_TOPO). Picture illustrating the deforestation process with the conversion of forest into an intensive monoculture of banana (**Left**). Photo credit: (O. Evrard, September 2021).

the decline of traditional Mayotte garden (15%), with instead the development of monocultures of cassava or banana plantations (4% in 2003 to 21% in 2022). Cassava and banana monocultures are found on steep slopes (20%), with soils left bare under the crops. The erosion rates measured in experimental plots on the Dzoumogné catchment are much higher in intensively cultivated land (17 Mg ha year^{-1} on banana, 29 Mg ha year^{-1} on cassava) than under traditional farming (1.3 Mg ha year^{-1}) (*11*). The land use changes affecting this catchment showed a strong temporal heterogeneity, with a relative stability of land uses between 2003 and 2012 and then strong changes between 2012 and 2022. These changes can be explained by the construction of an unpaved road in 2014 across the catchment and facilitating the access to the fields for farmers across a wider area. This road contributed to the fragmentation of the landscape following the intensification of agriculture and facilitated the transport of agricultural products to the villages. This catchment affected by land use change drains into the Dzoumogné reservoir (22 ha, average water depth of 8.5 m), one of the two reservoirs supplying drinking water to the island. It is affected nowadays by a reduction in water quality (i.e., cyanobacterial blooms and manganese contamination) and storage capacity due to reservoir siltation.

Recent global publications have emphasized the need to conduct local studies to evaluate the response of terrestrial and aquatic ecosystems to these increased anthropogenic pressures (*4*). Accordingly, Mayotte Island represents a worst-case example of human-environment interactions in the context of major land use changes and overpopulation that took place within 10 to 20 years. Understanding the mechanisms and trajectories of land and biodiversity evolution during the past decade on this island provides therefore an opportunity to monitor and report the dynamics of the ecosystem response to multiple increasing pressures. This should help to guide political decisions and/or conservation strategies in tropical islands (*12*). Collecting and analyzing sediment accumulated in reservoirs (e.g., lake and dam) represents a powerful tool for retrospectively reconstructing the trajectories of land and water resources and biological communities in the absence of long-term (>10 years) monitoring or field observations, at the catchment scale (e.g., suspended sediment and ecological census), which is a meaningful scale to manage land and water resources (*13*, *14*). These natural archives were already used to reconstruct sediment dynamics, erosion rates, and the sources of sediment in tropical conditions during time periods comprised between several decades and several millennia (*15*). Nevertheless, the combination of such a paleoenvironmental reconstruction associated with metabarcoding sedimentary DNA (*Sed*DNA) to evaluate changes in biodiversity has been very rarely implemented in tropical environments in general, and in Africa in particular (*16*, *17*). This technique was mainly applied in cold high-altitude and -latitude lake systems of Northern Europe and Northern America where conservation of ancient DNA is expected to be optimal to retrieve information on past biodiversity (e.g., plants, mammals, and lake biota) (*18*–*21*). According to Von Eggers *et al.* (*16*), only five studies have analyzed *Sed*DNA in

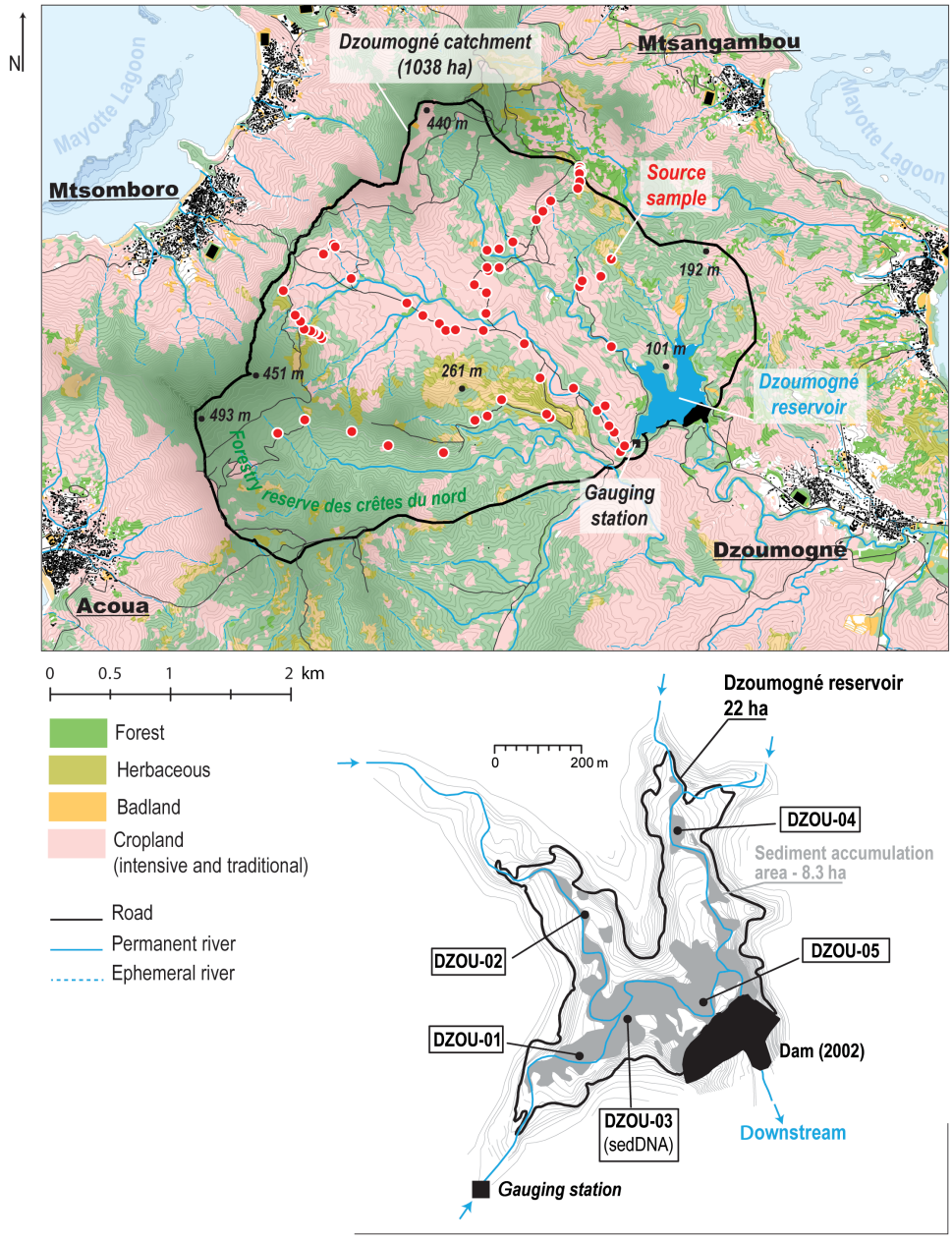

Fig. 2. Dzoumogné catchment and sampling locations. (**Top**) Simplified land cover map of the Dzoumogné catchment in 2018 and localization of the sediment sources collected for implementing the sediment fingerprinting approach. Localization of the sediment cores collected within the sediment accumulation area of the Dzoumogné reservoir (**Bottom**) (sources IGN, BD TOPO, and land cover from KERMAP).

African lakes, again mainly in high-altitude environments (*17*, *22*, *23*). The likely higher DNA degradation in warm tropical regions may limit the potential use of *Sed*DNA analyses in these areas as often only short segments of genetic material remain (*17*, *24*–*26*). However, pioneer studies have demonstrated that protocol optimization can improve environmental DNA detection in tropical soil and sediment material (*27*, *28*).

To address this lack of data in lakes of tropical environments, the current research provides an original approach combining these improved DNA detection techniques along with other reference methods (e.g., geochemical tracing) applied to the sediment accumulated in the Dzoumogné reservoir. The goals of this study were:

(i) To reconstruct the evolution of soil erosion rates based on the quantification and characterization of the volume of sediment accumulated within the reservoir, combining the use of sediment cores and bathymetric surveys;

(ii) To identify the main sources of land degradation including sediment originating from forests, cultivated land, and subsoil sources (e.g., bank erosion and badlands) by developing an original sediment fingerprinting approach comparing the properties (e.g., organic matter

properties, geochemistry, and color) of the sediment accumulated in the reservoir to those of the main land use sources.

(iii) Last, to reconstruct the response of different biological communities (e.g., plants, mammals, and eukaryotes) to these anthropogenic pressures by using *Sed*DNA analyses along one of the sediment cores.

This study will provide us with an original body of data for proposing integrated management methods aimed to limit the harmful consequences of rapid population growth in an area with limited natural resources.

RESULTS

Core description and chronology

The five sediment cores collected in the Dzoumogné reservoir ranged between 23 and 41 cm in length. The DZOU-05 sequence (36 cm long), collected close to the dam was defined as the master sequence for this study. This core consisted of alternating pluricentimeter–size ochre layers and millimeter-size dark layers. The organic fraction represented only a small proportion of the total accumulated material (including both autochthonous and allochthonous inputs). In this sequence, the average TOC (total organic carbon) reached 4.0 ± 1.6% with a maximal value of 9.7% in the dark layer located on the top of the core (0- to 1.5-cm depth). The lowest values were recorded in ochre layers (e.g., 2.3% between 25.5- and 26-cm depth). The C:N (Carbon:Nitrogen ratio) values were homogenous from the top to the bottom of the core with an average value of 11.3 ± 1.3. A monomodal distribution of particle sizes was observed all along the core with an average median size (*d*50) of 10.8 ± 5 μm (Fig. 4). Similar sedimentological observations were made for the other sediment sequences collected within the Dzoumogné reservoir. Only the sediment archives collected in the deltaic areas of the tributaries flowing into the reservoir were characterized by a coarser particle size in comparison with the two cores collected in the vicinity of the dam (i.e., average *d*50 of 42 ± 30, 150 ± 110, and 51 ± 42 μm for the DZOU-01, DZOU-02, and DZOU-04 cores, respectively). No specific trend of $^{210}Pb_{xs}$ activity was observed on the DZOU-05 sequence as in the other cores. The maximal $^{210}Pb_{xs}$ activity was detected between 15- and 16-cm depth (92 Bq kg^{-1}) and the minimal between 25 and 26 cm depth (16 Bq kg^{-1}), with an average activity around 48 ± 20 Bq kg^{-1}.

In the absence of continuous $^{210}Pb_{xs}$ decay ($r^2 < 0.1$) along the core, the sedimentation chronology was established by interpreting the alternation of ochre and dark layers at the light of our knowledge of sediment dynamics in this catchment. The climate of Mayotte Island is characterized by an alternation of pronounced dry and humid seasons (typically from December to March), promoting alternatively the accumulation of autochthonous matter during low flow periods and terrigenous sediment generated by erosion processes triggered during the wet season. The ochre layers, a color typical of that of the island soils, with high terrigenous contents and coarser particle sizes (depending on the individual core location) were associated with the sediment transported during wet seasons. Conversely, the millimeter-size dark layers were associated with the dry seasons characterized by low sediment inputs and the high production of autochthonous organic matter. The age model was established by correlating temporal series from the meteorological data (rainfall) measured at the M'tsamboro station (≈4 km from the Dzoumogné reservoir) with the terrigenous proxies extracted from the x-ray fluorescence (XRF) core scanner analyses (i.e., described in Materials and Methods) (fig. S1). This age model was computed by correlating the beginning and the end of humid seasons with the fluctuations of titanium (count numbers), associated with sediment delivery. The DZOU-05 sequence spans an 11-year period (ranging between 2011 and 2021) with an average sedimentation rate (SR) of 5.6 cm year^{-1} (SR was ranging between 4.4 to 6.5 cm year^{-1} within the five cores). The highest SRs were recorded in this core during the 2019–2020 and 2020–2021 humid seasons (9 and 9.5 cm year^{-1}, respectively), whereas the lowest sedimentation was observed during the 2017–2018 humid season (2 cm year^{-1}), corresponding to a historical drought.

Reservoir siltation and origin of the sediment

The volume of sediment accumulated in the Dzoumogné reservoir increased by 180% between 2011 and 2021 during two periods of important sediment delivery (Fig. 3). A first acceleration with a 240% increase of sediment accumulation was recorded between 2011 and 2015 [moving from 1500 tonnes year^{-1} (SD 500 tonnes year^{-1}, SD associated with the volume estimation) in 2011 to 5100 tonnes year^{-1} (SD 3000 tonnes year^{-1}) in 2015], followed by a second 160% increase between 2019 and 2021 [moving from 1600 tonnes year^{-1} (SD 600 tonnes year^{-1}) in 2019 to 4200 tonnes year^{-1} (SD 2500 tonnes year^{-1}) in 2021]. In 10 years, approximately 25,000 tonnes (SD 14,000 tonnes) of sediment were stored in this reservoir.

Sediment fingerprinting results demonstrated that on average, 62% (SD 8%) of the sediment accumulated in the Dzoumogné reservoir between 2011 and 2021 originated from subsoil sources (e.g., bank erosion, badlands, gully erosion, and channel bank collapse within the reservoir) followed by cropland (28%, SD 7%) and forest sources (10%, SD 2%) (Fig. 3). The highest cropland contributions were observed in 2013–2014 [average contribution of 34% (SD 25%) and in 2019–2020 [average contribution of 38% (SD 26%)]. In contrast, the highest subsurface and forest contributions were recorded between 2015 and 2018 [on average 73% (SD 19%)] and in 2019–2020 [on average 15% (SD 13%)] (Fig. 3). Multivariate series analyses based on principal components analysis (PCA) were able to identify three breakpoints in the sediment source time series at the end of 2011 (confidence interval 2011.9 to 2012.1), end of 2014 (confidence interval 2014.6 to 2015), and at the end of 2018 (confidence interval 2018.7 to 2019.1), respectively.

Evolution of erosion rates

In 10 years, average erosion has increased by 130%, rising from 1.2 Mg ha year^{-1} (SD 0.9 Mg ha year^{-1}, SD associated to erosion reconstruction) in 2011 to 2.8 Mg ha year^{-1} (SD 1.4 Mg ha year^{-1}) in 2021 (Fig. 3). During this period, two main acceleration phases of erosion were observed during the 2011–2015 and the 2019–2021 periods. The highest erosion rates were recorded during the rainy season 2015 [4.9 Mg ha^{-1} year^{-1} (SD 2.8 Mg ha^{-1} year^{-1})] and 2021 [2.8 Mg ha^{-1} year^{-1} (SD 1.4 Mg ha^{-1} year^{-1})], whereas the lowest erosion rates were observed between 2017 [0.4 Mg ha^{-1} year^{-1} (SD 0.2 Mg ha^{-1} year^{-1}) and 2019 (0.9 Mg ha^{-1} year^{-1} (SD 0.5 Mg ha^{-1} year^{-1})] (Fig. 3). The use of univariate AMOC (analyzing means of counts) method was able to identify three breaking points in this temporal series at the end of 2011, in mid-2016, and at the end of 2019.

OTU richness and taxonomic composition

A total of 766 unique operational taxonomic units (OTUs) were detected along the sediment core analyzed for DNA (core DZOU-03). The sum of reads [defined as the number of base pairs (bp) sequenced

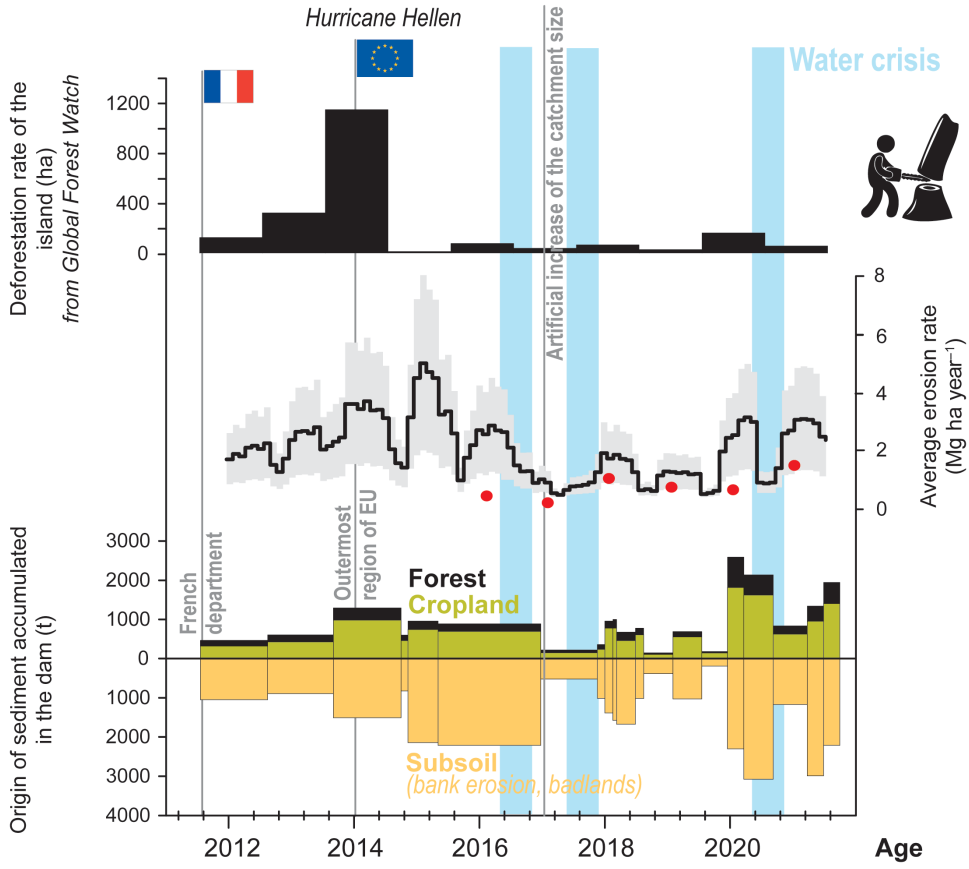

Fig. 3. Trajectory of soil erosion and sediment sources on Dzoumogné catchment. Evolution of the deforestation rate on Mayotte Island (**Top**), trajectory of erosion rates (the gray area corresponds to the uncertainty) (**Middle**), and origin of the volume of sediment accumulated within the Dzoumogné reservoir with the respective contributions of forest, subsoil (e.g., bank erosion and badland), and cropland sources (**Bottom**). The red dots represent soil erosion rates reconstructed using the river gauging records (Fig. 2) for one of the sub-basins draining to the reservoir (*11*). The blue areas correspond to the water crises occurring during austral summers. The years 2011 and 2014 correspond to changes in the administrative status of the island becoming a French department in its own right and an outermost region of the European Union.

from a DNA fragment] per sample increase from 678,000 reads in 2011 to 4,500,000 reads in 2016 and 1,450,000 at the top of the core, in 2021. The number of OTUs varied from 72 to 394 per layer from the base to the top of the core. The number of OTUs increased by 450% between 2011 and 2021. These OTUs were assigned to 23 taxonomic groups. The *Metazoa* taxonomic group dominated the OTUs richness with 25% (SD 9%) of the OTUs detected in the Dzoumogné reservoir followed by the *Streptophyta* [23% (SD 10%)], the *Fungi* [18% (SD 3%)], the *Alveolata* [11% (SD 3%)], and the *Euglenozoa* and *Rhizaria* taxonomic groups [7% (SD 1.5%), and 5% (SD 3%), respectively]. Twelve OTUs were persistent thoughout the time series (detected in the 12 samples) (Fig. 4).

The number of positive replicates was used in this study to evaluate the relative abundance of the OTUs within the core (*29*). A total of 202 orders were detected within the seven most abundant taxonomic groups mentioned above. Among them, 15 orders explain 30% of the abundance detected in the core. The most abundant orders were *Eulglenida* (Eucaryote: 30 unique OTUs, 361 positive replicates), *Fabales* (Plantae: 24 unique OTUs, 112 positive replicates), *Sapindales* (Plantae: 13 unique OTUs, 102 positive replicates), *Ebriida* (Eucaryote), *Polyporales* (Fungi), *Spathiida* (Animalia), *Ploima* (Animalia), *Eurotiales* (Fungi), *Cyprinodontiformes* (Animalia), *Rosales* (Plantae), *Lamiales* (Plantae), *Hypocreales* (Fungi), *Agaricales* (Fungi), *Pleosporales* (Fungi), and *Caryophyllales* (Plantae) (Fig. 4). The trajectories of the relative abundance of the main orders ($n = 73$) is provided in the Supplementary Materials (figs. S4 to S8).

Source of terrestrial DNA

Abundance of terrestrial communities was mostly associated with the changes of *Streptophyta* taxonomic group, in terms of both abundance and diversity (fig. S7). This group was composed of 38 orders. Among them, 37 were characteristic of terrestrial habitats. In addition, of the 40 orders of *Fungi*, 13 were exclusively originated from terrestrial environments (65% of the total abundance) (fig. S5). These orders were dominated by the *Agaricales*, *Hypocreales*, or again, *Polyporales* with 43, 47, and 52 positive replicates, respectively (Fig. 5). These orders appeared in the sequence after 2014 or have seen their relative abundance increasing after this period. Changes in terrestrial habitat communities were also highlighted with the detection of some orders from the *Metazoa* taxonomic group (fig. S6), such as the *Primates* or the *Hemiptera* orders, for which the detection started after 2013 and 2014, respectively (8 and 14 positive replicates). Some soil organisms such as terrestrial worms also demonstrated an increase of detection throughout time (*Crassiclitellata* and *Aporcelaimidae* orders). These two orders were already detected at the base of the core but have seen

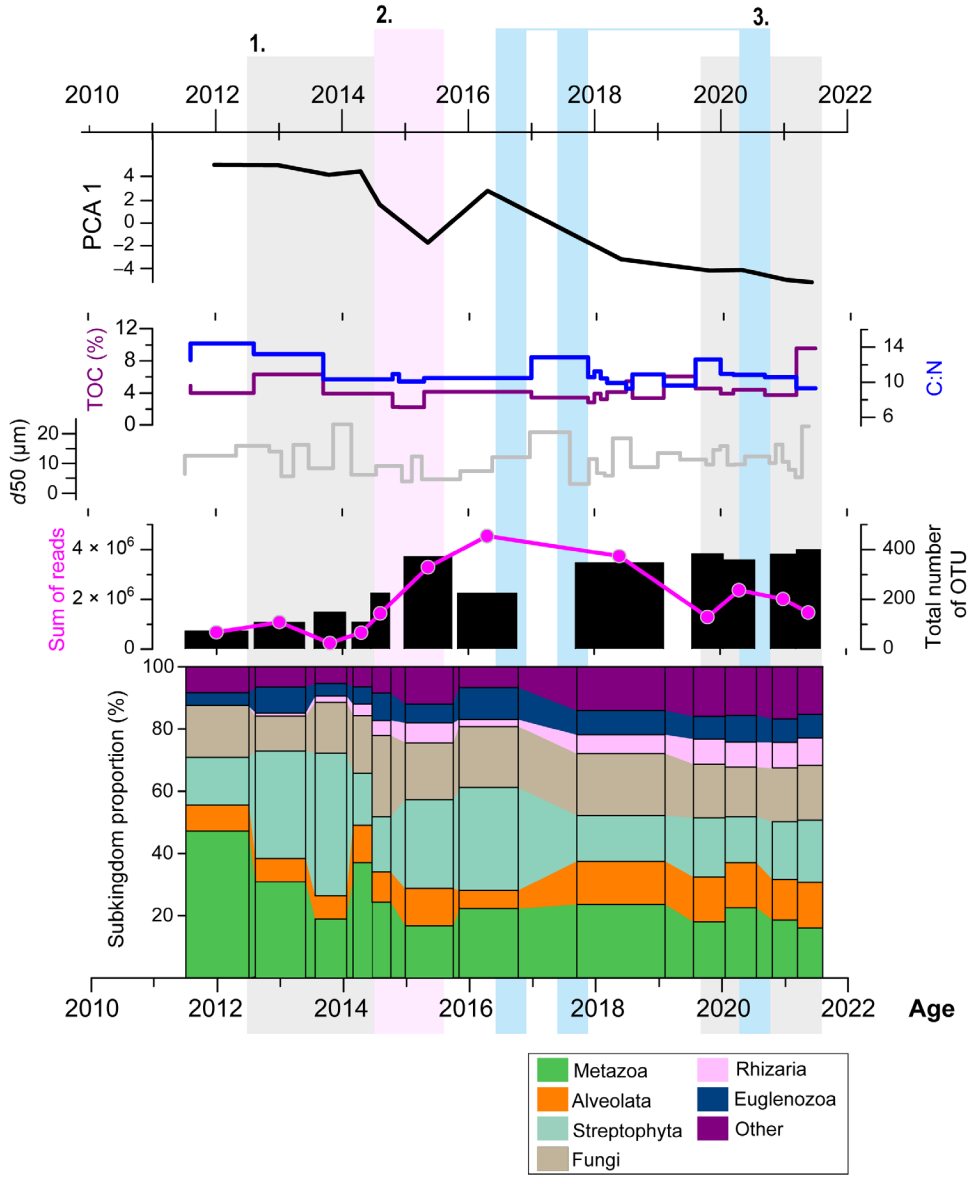

Fig. 4. Taxonomic composition and sediment properties. Evolution of the proportion of the taxonomic groups, number of operational taxonomic units (OTU), sum of the reads in comparison to the average particle size (*d*50), organic content (TOC%), and organic origin (carbon/nitrogen ratio C:N) in the sediment core. PCA1 (axis 1 of the PCA) represents the result of multivariate series analyses identifying the breakpoints in the *Sed*DNA communities. The gray stripes (1) correspond to the deforestation period, the pink stripe (2) to the major episode of landscape fragmentation, and the blue stripes (3) to the main water crisis periods.

their abundance increasing throughout time [e.g., *Crassiclitellata* was detected in average in 1.5 replicates per level at the exception of the level deposited after 2020, demonstrating a greater detection (i.e., 10 positives replicates)]. The same observation was made for some soil protists detected after 2014 and demonstrating greater abundance between the 2014–2015 and 2019–2021 periods (*Plasmodiophorida* order) (Fig. 5).

Agriculture-based DNA

Food-producing agricultural systems (traditional or intensive) are mainly based on banana or cassava cultivation in Mayotte Island (90% of the island's cultivated area). The *Zingiberales* order to which the *Musaceae* family belongs was detected in 5 layers (11 positive replicates and in 6 positive replicates for the *Musaceae* family) (Fig. 6). This family was detected almost all along the core with the exception of the post-2020 period, where it was found in relatively low abundance. The cassava, belonging to the *Euphorbiaceae* family (*Euphorbiales* order), was detected in 4 layers and 10 positive replicates. This family was the most abundant during the 2013–2015 period. After 2017, this family was only detected in one sample and replicate. These agricultural systems are supplemented by more specialized systems such as mango, papaya, guava, coconut, breadfruit, and, to a lesser extent, market gardening (*8*). The families to which these species belong were all detected in the core with very contrasting trajectories (Fig. 6). Mango was observed all along

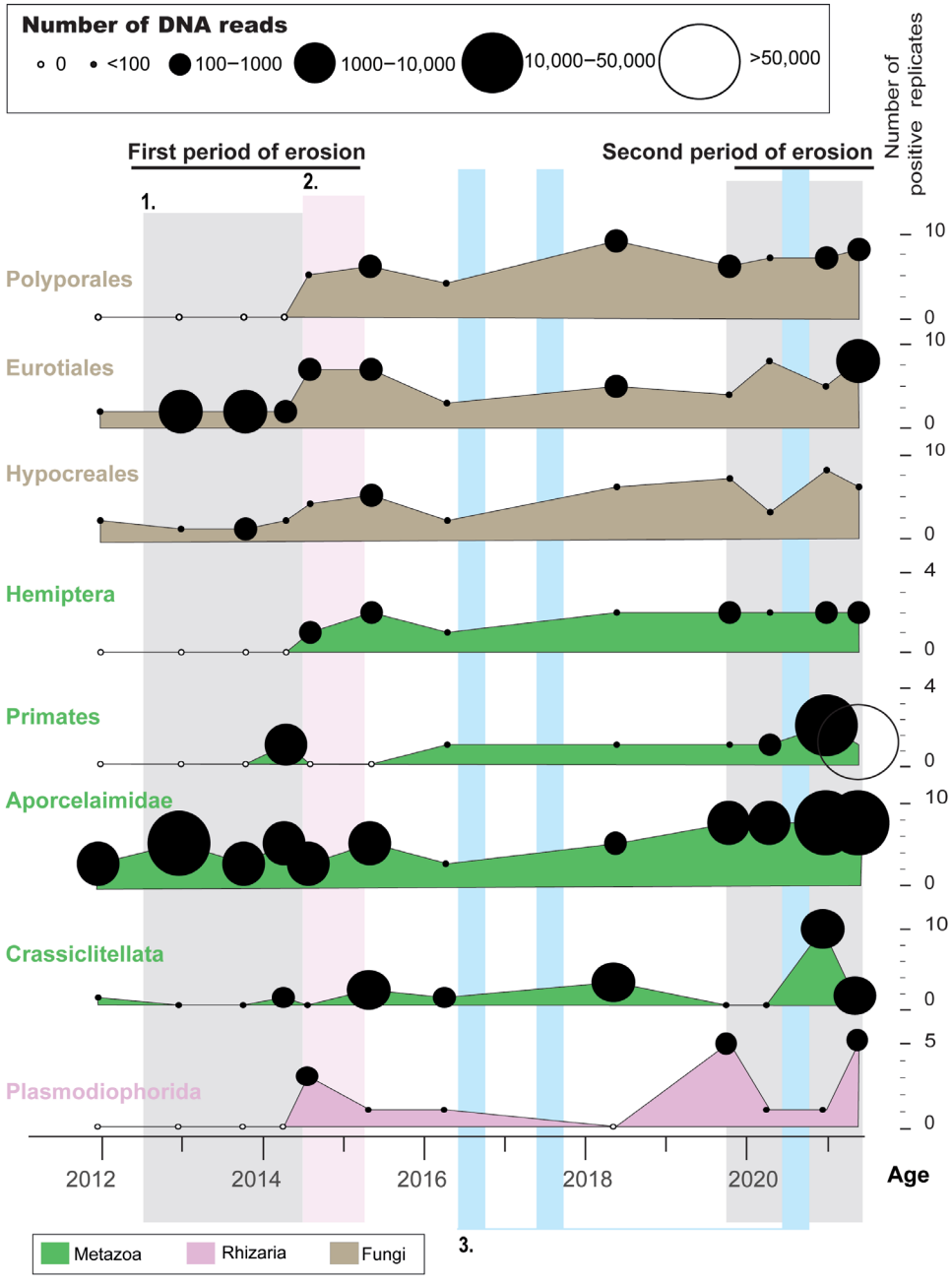

Fig. 5. Responses of terrestrial communities to landscape fragmentation. Evolution of the relative abundance of orders belonging to Fungi, Metazoa, and Rhizaria taxonomic groups. The size of the circle is proportional to the number of reads. The gray stripes (1) correspond to the deforestation periods, the pink stripe (2) to the main episode of landscape fragmentation, and the blue stripes (3) to the main water crisis periods.

the sequence with a greater detection after 2015 (56 of the 61 positive replicates of the *Anacardiaceae* family were assigned to the *Mangifera* genus during this late period), papaya in 8 layers (8 of the 12 positive replicates of the *Caricaceae* family were assignated to the *Carica* genus), and guava in 2 layers after 2020 (3 positive replicate of the *Myrtaceae* family). The coconut family was observed in 4 layers (6 of the positive replicated of the *Arecaceae*, no genus assignation) that all took place between 2012 and 2016, and the breadfruit family was detected all along the sequence with an increase of abundance after the 2014 and 2020 periods (21 of the 42 positive replicates of the *Moraceae* family were assignated to the *Artocarpus genus*). In Mayotte Island, cattle and sheep/goat breeding occurs in 25 and 16% of the farms, respectively (*8*). DNA from the *Artiodactyla* orders to which the *Bovidae* family belongs was detected in low relative abundance (eight positive replicates) in four levels between the 2014–2015 and 2016–2020 periods (Fig. 6).

Source of aquatic DNA

Most of the OTUs from the *Metazoa* taxonomic group detected in the sediment core belong to aquatic habitats. They were mostly dominated by two orders, the *Cyprinodontiformes* and *Cypriniformes*

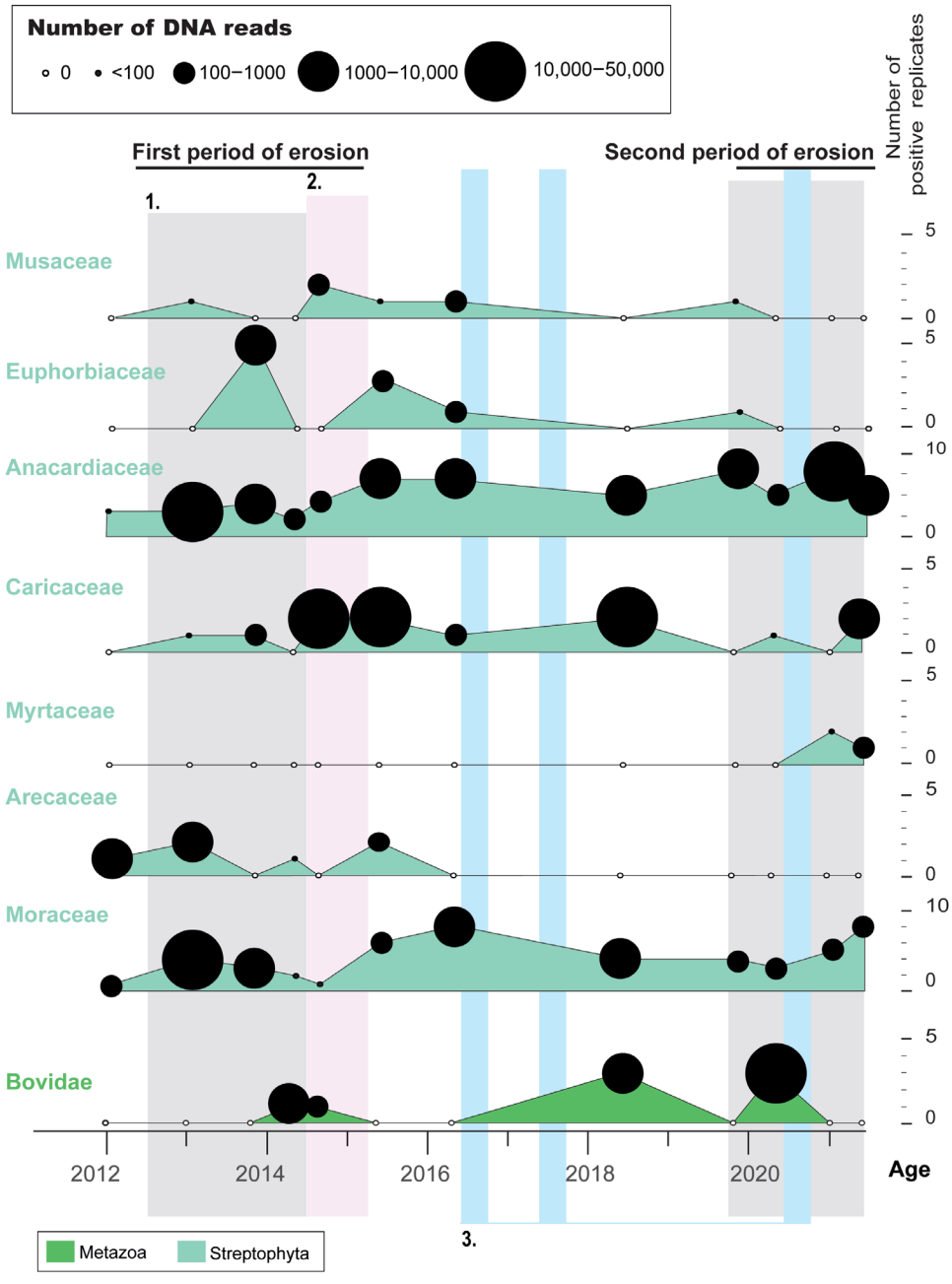

Fig. 6. Responses of agriculture-derived communities to agriculture intensification. Evolution of the relative abundance of the main cultivated families of the Dzoumogné catchment and associated cattle. The size of the circle is proportional to the number of reads. The gray stripes (1) correspond to the deforestation periods, the pink stripe (2) to the main episode of landscape fragmentation, and the blue stripes (3) to the main water crisis periods.

(freshwater fish detected in 67 and 40 positive replicates, respectively). These two orders of fish were detected all along the core, with a greater abundance after 2014. They follow the same trajectory as the *Cyclopoida* order, which appeared after 2014 with a maximal abundance after 2020 (Fig. 7). The aquatic environment was dominated by a large diversity of eukaryotes with OTUs belonging to the *Chlorophyta* taxonomic group. We could, for example, identify the appearance of the *Volvocales*, *Chlorellales*, and *Spathiliida* orders after 2014 and 2015, respectively. Some of them such as the *Chlamydomonadales*, *Volvocales*, and *Spathiliida* demonstrated an increase of their relative abundance in 2015 and after the 2020 period. The post-2014 period coincides also with the greater abundance of some *Euglenozoa* orders such as *Euglanes* and *Euglenida*, detected all along the sequence with an average relative abundance of 1 and 4 positive replicates before 2014 and 3 and 43 positive replicates after this year (Fig. 7).

Trends, temporal tipping point, and taxonomic structure

Multivariate series analyses based on PCA was able to identify two breakpoints in the temporal series in mid-2014 (confidence interval, 2014.3 to 2015.4) and in early 2016 (confidence interval, 2016.3 to

2019.8), respectively. After the first breakpoint, 94 OTUs that were not previously detected appeared and 140 after the second breakpoint (on average 66 unique OTU appeared in each sample). They were belonging mostly to the *Fungi*, *Metazoa*, and *Streptophyta* groups after the first breakpoint (39, 14, and 11%, respectively) and to the *Streptophyta*, *Fungi*, and *Alveolata* groups after the second one (22, 20, and 18%, respectively).

CONISS clustering allowed the detection of three main groups of samples with similar taxonomic assemblages. The first one is composed of four samples at the base of the core (group 3 between 2012 and 2014.3—deforestation period and acceleration of erosion), the second one is composed of two samples in the middle portion of the core (group 2 dated to 2014.6 and 2016.3—transition between the first erosion period and the water crisis), and the last one of the six samples mainly located at the top of the core (group 1 dated between 2018.4 and 2021.4—second period of acceleration of soil erosion—eutrophication processes) with the exception of the sample dated to 2015.6, also associated with this group (fig. S3).

The biodiversity indices performed on the different genetic markers show different trends of diversity before, during and after the period mentioned above (table S1). Taking the Shannon, Simpson, or Chao1 indices as an example for the "Balitzki_12S" (vertebrates), they were significantly higher after the 2019 period (group 1). These same indices demonstrated a decrease of Eucaryotes and Metazoa diversity for the period corresponding to the group 2 (2014.6-2018.4 with the exception of sample 2015.6), for the "Hardy_18S" and "Kelly_16S" genetic markers, respectively. For the plants and fungi genetic markers ("White_ITS" and "Prosser_rbcl"), these indices demonstrated a substantial increase of diversity during the 2013.8-2016.3 and 2019.8-2021 periods. This observation was more pronounced for "White_ITS" than "Prosser_rbcl."

Univariate analysis–based AMOC was applied to the 38 orders of the *Streptophyta* group to identify trends in the relative abundance (number of positive replicates). Thirty-one percent of them followed a positive trend (25% recorded a significant breakpoint). Results indicate that 13% of the 71 *Metazoa* orders also demonstrated a positive trend (breakpoint detected in 13%), 25% of the 40 *Fungi* orders (15% record breakpoint), 52% for the 33 order of *Alveolata* (breakpoints detected in 36%), 100% for the 3 *Euglenoza* orders (breakpoint between 2015.3 and 2016.3 for the 3 orders), and 25% for the 12 orders for the *Rhizaria* (breakpoint detected for 13% of the orders)—(statistical results for each order are provided in table S2).

Effects of environmental variables on community composition

We used multivariate analyses to investigate relationships between environmental variables (e.g., erosion rate, source contribution, cyanobacterial concentration, and meteorological data from the M'tsamboro station) and composition of the abovementioned orders. To assess the correlation between environmental variables and taxonomic composition, we performed RDA (redundancy analysis) and CCA (canonical correlation analysis) analyses, as described by Chen and Ficetola (*29*). The results of these analyses showed general trends in the relationships between environmental variables and taxonomic composition. However, no significant correlation was observed for any of the 202 orders examined.

To assess the statistical significance of the relationships between environmental variables and OTU composition, permutation tests were also performed. The results of these tests were that none of the environmental variables considered showed a significant effect on community composition. Last, a detailed analysis of the coefficients of the environmental variables in the RDA models confirmed that the environmental variables failed to influence taxonomic composition.

Our results suggest that variations in environmental variables are not strongly associated with changing community composition. These statistical methods examine relationships over a long period of time. It is possible that sudden events, such as a change in connectivity or an increase in deforestation causing a change in community, are not captured by these methods. It is also possible than the temporal resolution of our samples analyzed for DNA (yearly resolution) is not adapted to the resolution of our variables (e.g., weekly or daily for cyanobacterial blooms and meteorological data, respectively).

DISCUSSION

Mayotte Island represents a unique living laboratory to understand the anthropogenic and climatic interactions in a context of overpopulation and rapid demographic growth. During the past 10 years (2011 to 2021), these stressors have interacted with an unprecedented intensity inducing major social crises (e.g., water conflicts) and threatening the main components of the terrestrial and hydrological ecosystems of this island.

These stressor interactions have been exacerbated since 2011 and the change in the administrative status of Mayotte Island increasing anthropogenic pressures on natural resources. As a result, erosion rates were accelerated by 300% between 2011 and 2015 during the first deforestation period (increasing during the rainy season from 1.2 to 4.9 Mg ha^{-1} $year^{-1}$, respectively) and by 190% during the 2019–2021 period (moving from 0.9 Mg ha^{-1} $year^{-1}$ to 2.8 Mg ha^{-1} $year^{-1}$ between the 2018 and 2021 rainy seasons), mobilizing mainly the subsoil and cropland sources (Fig. 3). The highest erosion rate during the studied period was recorded during the rainy season 2014–2015 just after the creation of the unpaved road in the catchment and during the period of maximal deforestation observed in 2014 (loss of 1150 ha of forests at the island scale, including 28 ha in the Dzoumogné catchment), (www.globalforestwatch.org). This road was built all across the Dzoumogné catchment and greatly facilitated access for the expansion of agriculture at the expense of forests, as previously observed in Amazonia (*30*). By facilitating the transport of agricultural products to the neighboring village, it also encourages the intensification of agricultural practices at the expense of traditional farming. This intensive agriculture is based on both the practice of monoculture and the burning of vegetation residues on the soil to reduce the incidence of crop parasites and to facilitate access to the field. In this intensive farming system, the soils are left bare and vulnerable to erosion. In a systematic review of soil erosion in the humid tropics, Labrière *et al.* (*31*) highlighted that the creation of bare soil patches within the landscape dramatically increases soil erosion. The authors recorded an average soil loss of 15.5 Mg ha^{-1} $year^{-1}$ under bare soil [17 to 29 Mg ha^{-1} $year^{-1}$ were measured in experimental plots of the Dzoumogné catchment (*11*)] in comparison to 0.1 Mg ha^{-1} $year^{-1}$ under forested lands). The landscape fragmentation associated with deforestation and agriculture intensification processes may explain the acceleration of erosion during this period (*31*). In addition, the occurrence of tropical hurricane *Hellen* at the end of the 2013–2014 rainy season resulted in historically abundant rainfall (275 mm in 2 days recorded 2 km away from

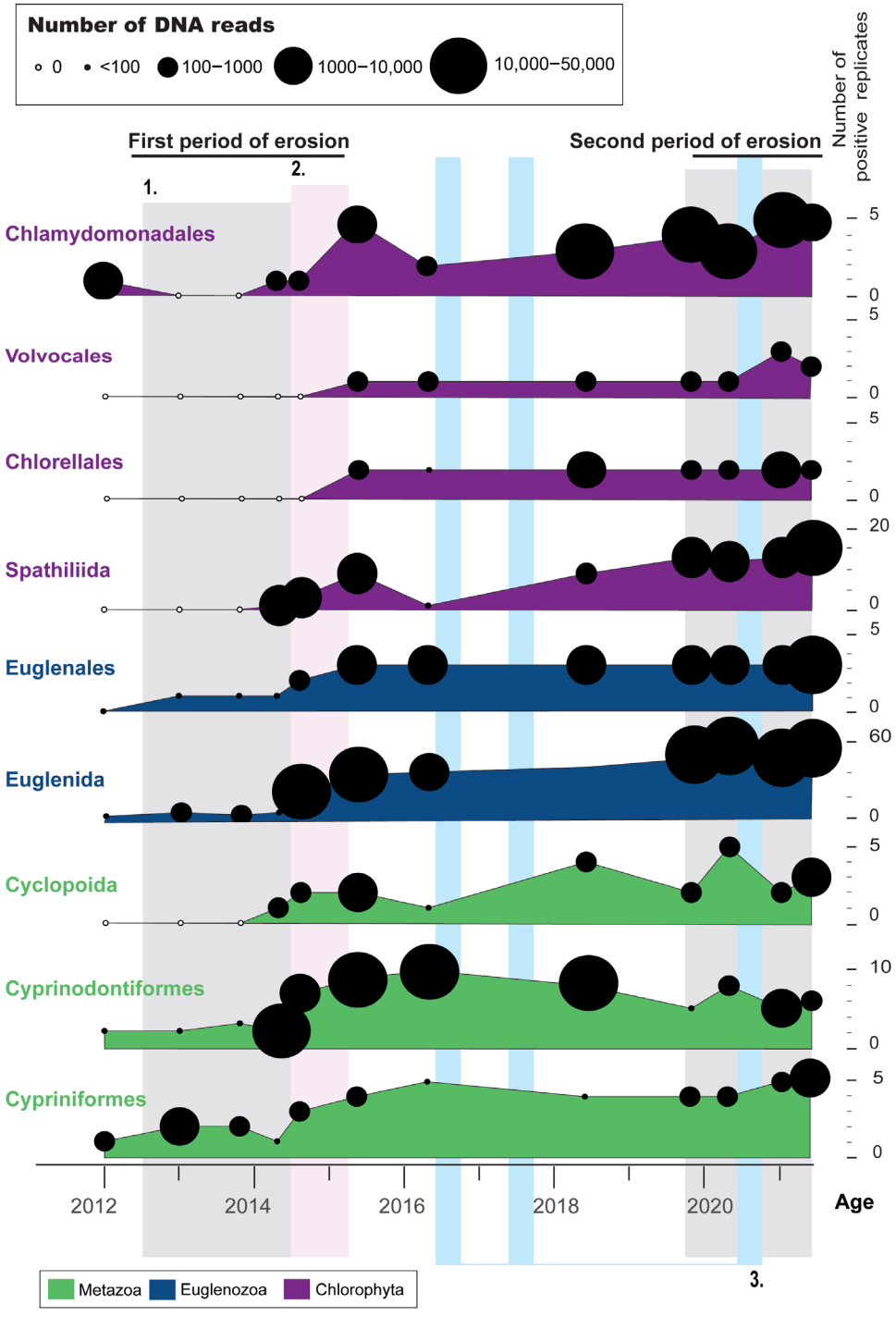

Fig. 7. Responses of aquatic communities to anthropogenic and climatic stressors. Evolution of the relative abundance of orders from the Metazoa, Euglenozoa, and Chlorophyta taxonomic groups. The size of the circle is proportional to the number of reads. The gray stripes (1) correspond to the deforestation periods, the pink stripe (2) to the main episode landscape fragmentation, and the blue stripes (3) to the main water crisis periods.

the Dzoumogné reservoir, in Mtsamboro Village; Fig. 2) on land affected by this conversion. The occurrence of this event has generated the second highest erosion rate recorded during the 2011–2021 period (3.6 Mg ha^{-1} year^{-1}). Erosion of the unpaved road, degraded cultivated soil, and the channel bank collapse of the reservoir during this hurricane may explain the particularly high contribution of subsoil sources to sediment (71%) during this period (Fig. 3) (*32*). The second period of intense soil erosion (2019–2021) took place during a recent phase of conversion of agricultural practices under sustained migratory and demographic pressures. As between 2011 and 2015, this period underlines the disappearance of traditional practices and fragmentation of the landscape (i.e., intensive agriculture

represented 15% of the cultivated area in the catchment in 2003 and more than 50% in 2021) during a latest phase of deforestation at the scale of Mayotte Island [i.e., loss of 167 ha of forests at the island scale in 2020 (www.globalforestwatch.org)] despite being less extensive than the first phase recorded between 2012 and 2015. The erosion values recorded after 2017 were probably underestimated. After the 2016 water crisis, the catchment size was artificially increased to accelerate replenishment of water into the reservoir, changing from 724 to 1038 ha and draining a forested sub-catchment (the forest reserve of "*les crêtes du nord*", Fig. 2). The catchment surface has increased by 43% through draining an additional sub-catchment with a low sediment production reducing artificially the erosion rate (i.e., catchment size is a key component for the reconstruction of erosion rates based on paleo-environmental approaches; see Materials and Methods). Erosion should amount to around 4.2 Mg ha^{-1} $year^{-1}$ in 2021, without taking into account sediment production in this artificially captured sub-catchment. Values obtained in this study are in the same order of magnitude as those reconstructed using the gauging station draining one of the sub-catchments of the Dzoumogné reservoir (*33*)—(i.e., the difference in the values can be explained by the difference in the land uses observed between this sub-catchment and those in the whole catchment and by the fact that the bedload was not measured at the gauging stations) (Figs. 2 and 3). It is also similar to global erosion model outputs for this world's region [e.g., average erosion of 3.88 Mg ha^{-1} $year^{-1}$ (*34*)] although lower than the erosion rates measured on the neighboring and highly degraded Madagascar island (i.e., low vegetation cover and intensive erosion processes) where erosion rates between 200 and 400 Mg ha^{-1} $year^{-1}$ have been reported (*35*, *36*).

*Sed*DNA results showed major changes in the number of species detected and biological communities observed before, during, and after the first erosion period (2011–2015) and to a lesser extent, after the second erosion phase (2019–2021), (Fig. 4). These important changes can be explained by a greater supply of DNA derived from the terrestrial environment following landscape fragmentation or by the degradation of DNA over time (*37*). This degradation may cause a shift in fragment size, with a greater detection of less fragmented DNA in the top of the core, according to the length of DNA targeted in this study. Paleo-environmental studies using ancient sedimentary DNA (*Seda*DNA) spanning several millennia and targeting degraded DNA consist mainly of DNA reads between 30 and 100 bp although some research has found fragments >500 bp in Holocene records [e.g., (*34*)] according to Capo *et al.* (*13*). We believe that the DNA preservation conditions of the Dzoumogné reservoir and the timescale targeted by our study (10 years compared to several millennia for *Seda*DNA) provide confidence that we are recording a shift in communities instead of a shift in DNA fragment size. These conditions include fine silt sediment ($d50$ of 10.8 ± 5 μm), dominance of homogenous organic contents from terrestrial origin [C:N of 11.3 ± 1.2 (*38*)], high SRs (>5 cm $year^{-1}$), high connectivity from sources to the reservoir, and anoxic conditions at the sediment surface. Our protocol optimization, which mixes the use of multiple barcodes of different lengths (e.g., three genetic markers ranging from 50 to 380 bp were used for plants), further supports this conclusion. Our hypothesis is supported by our results evaluating the DNA degradation by comparing the impact of sequence lengths on the number of reads obtained (table S3).

Accordingly, erosion induced by deforestation, agriculture, and landscape fragmentation processes has induced a greater diversity of DNA before and after the first erosion period. This hypothesis is supported by the shift in abundance and diversity of communities, the greater detection of OTUs, and the identification of groups of samples before and after this period (Fig. 4 and fig. S3).

The impact of erosion processes—landscape connectivity on the change in DNA sources or taxonomic groups (e.g. mobilizing different soil horizons, mobilization of specific sources)—was reported in previous *Sed*DNA studies (*13*, *37*). These results further demonstrate the potential of *Sed*DNA to reflect the intensity of ecosystem disturbance. The sudden increase of detection of OTUs belonging to terrestrial habitats after the first erosion phase supports this observation (Fig. 5). After this landscape fragmentation and increase of landscape connectivity, soil organisms and microorganisms start to be detected or their detection start to statistically increase for some of them in the Dzoumogné reservoir sediment. Among them, soil *Fungi*–derived orders appeared or showed an increase in relative abundance, and for most of them, as for the *Polyporales*, *Eurotidales*, *Hypocreales*, *Agaricales*, *Pleosporales*, and *Sordariales*, a statistical jump in the time series synchronous of the two erosion phases. These orders include primary terrestrial *Fungi* taxa that are found in a variety of terrestrial environments, such as wood-decay fungi, plant debris fungi, plant and insect pathogens, and some species of mycorrhizal fungi that grow together with trees, soil, and plants. Other soil organisms demonstrated the same trajectory of appearance or increasing detection such as the *Crassiclitellata* (an order of annelids including earthworms), the *Aporcelaimidae* (an order of nematode living in the soil), or *Monhysterida* (an order of nemadote found in soil and freshwater). The detection of certain terrestrial protists from the *Plasmodiophorida* order (belonging to the *Rhizaria* taxonomic group), plant parasites found in the soil, occurred during the same periods. As for the fungi and nematode orders, the terrestrial protists started to be detected after the first period of erosion and their relative abundance increased statistically after 2014. Microorganisms, fungi, and nematodes are fundamental components of soil biodiversity (*35*). Previous studies have reported the impact of soil erosion on the decline of fungal richness in both topsoil and subsoil layers (*36*). Changes in terrestrial Fungi communities were previously used for tracking catchment dynamics related to environmental disturbance (e.g., land use change) by analyzing the fungal communities recorded in lake sediments (*39*). The increase of diversity of these organisms and microorganisms in reservoir sediment, which is synchronous to landscape fragmentation, give an insight into the intensity of erosion processes mobilizing a large community of organisms from soil habitats and supplying them to the lake (Fig. 5).

As a result of the increased connection of the forest habitat with the river network and—ultimately—the reservoir, several emblematic families belonging to the order of *Primates* started to be detected in the sediment core, such as the *Lemuridae* family or *Lemure* taxa, arboreal native species of the Comoros island, which were only detected after 2014. This is also the case for the *Hemiptera* order, one of the largest orders of insects living mainly in contrasted terrestrial environments (e.g., forest, cultivated land, and wetland), which also started to be detected after 2014 (Fig. 5). This period of increase in connectivity was also accompanied by a greater abundance and richness of terrestrial plants. Among them, the *Fabales*, *Sapindales*, *Rosales*, or *Lamiales* (orders of flowering plants found in diverse environments including forest, grassland, and cultivated land) were the most abundant orders of *Streptophyta* detected in the core. They exacerbate a positive trend in detection observed from the base to

the top of the core with a further statistic jump after the first period of erosion. The additional detection of some families mostly found under forests likely further demonstrates the increased connection intensity between these forests and the river network. This is observed for the *Apocynaceae* and *Bignoniaceae* families (families of liana-type climbing plants) or *Dryopteridaceae* (a family of terrestrial ferns) detected in the core after 2013 and 2020, respectively.

The intensification of agriculture and the resulting changes in the erosion regime also led to an increase in the abundance of agriculture-related species. The main cultivated plants or those used for agricultural purposes were detected. As an example, *Sed*DNA allowed the detection of *Arecacea* family (family of coconut tree, detected only at the base of the core between 2012 and 2016), mostly cultivated in traditional Mayotte gardens. The detection of this family only during the first erosion period can highlight the conversion of these traditional practices into intensive farming. The breadfruit tree, the jackfruit tree, and Mango tree, belonging to the *Moracea* and *Anacardiaceae* families were detected all along the sediment core, with a statistical increase of their relative abundance after 2015. These two families along with the *Fabaceae* family (also known as the *Leguminosae* family, one of the largest families of flowering plants) were the most abundant families of plants detected in this sedimentary sequence. *Sed*DNA also allowed the detection of the *Euphorbiaceae* (family of the cassava) and the *Musaceae* families (including banana trees), both cultivated on bare soils—that are more vulnerable to erosion—with their abundance increasing during the first phase of erosion (Fig. 6). The low detection of these species can be explained by different factors. Part of these crops is exported for consumption, and the crop residues are often burned by farmers during the dry season. These crops also cause very rapid topsoil degradation through triggering important subsurface erosion processes (as highlighted by the sediment tracing results). The low detection rate can therefore probably be explained by a combination of these two factors, i.e., the low abundance of crop residues left on soils and a dilution of the topsoil DNA signal with a greater subsoil contribution depleted in DNA. The detection of some *Metazoa* related to the forest habitat or introduced by humans for agriculture also started to be detected after this first period of erosion. In particular, the presence of humans was mainly detected in two sediment layers attributed to 2014 and 2021 (detection of *Hominidae* taxa in four replicates). As no human settlement is found in the catchment, this human detection is likely mainly associated with agricultural activities. Human agricultural activities have occurred continuously between 2012 and 2021. However, the fact that this species was only detected during periods of maximum erosion supports again the role of erosion processes in the transfer of DNA from the sources of production. Agriculture-derived species were also identified with the detection of the *Cetartiodactyla* and *Artiodactyla* orders (mainly dominated by the *Bos* and *Bovinae* taxa). These man-bred species used by farmers were only detected in the uppermost part of core between 2018 and 2021 (Fig. 6).

Of note, the second phase of acceleration of erosion was less important in terms of change of biological communities, most likely because the main connectivity changes were initiated during the first period and only reactivated during the second phase. Nevertheless, the beginning of this second period of erosion was also associated with a statistical shift in some biological communities, sediment sources, and erosion dynamics. Sediment tracing results indicated the occurrence of a greater contribution of the forest source to reservoir sediment during this period, suggesting a greater pressure on forest sources with the accelerated transport of particles with a forest signature to the reservoir (*6*) and the greater detection of forest-derived species with DNA results (e.g., *Gentianales*, *Magnoliales*, *Asterales*, and *Malpighiales*). These DNA results emphasize the need for future *Sed*DNA studies aimed at reconstructing past biodiversity dynamics to consider the possible effects of physical changes (e.g., connectivity, sediment sources, and erosion dynamics) in sediment transport that may cause increases in recorded biodiversity that might otherwise be misattributed to other environmental drivers (e.g., climate change and anthropogenic pressures).

Less climate stress explains the decrease of erosion rates during the 2015–2019 period. The intensity of anthropogenic activities did not diminish, but scarcity and decrease in rainfall during this long period affected the level of water filling in the Dzoumogné reservoir. The siltation of the reservoir with sediment after the first main erosion period (2011–2015) and the low water capacity stored associated with the increase of water demand on the island induced by the demographic increase plunged the island into a major water crisis during austral summers (Fig. 2). The water restrictions induced by the lack of water caused a real deterioration in the health status of the inhabitants who were deprived of clean water and increased the socio-environmental pressures on water resources (*40*). The decrease of water level in the reservoir after this accelerated period of sediment delivery coincided with a change in aquatic communities (Fig. 7). *Sed*DNA results indicate the greater abundance or the detection of communities belonging to the *Chlorophyta* taxonomic group (also known as green algae) during this decrease of water level. Species belonging to the *Chlorellales*, *Volvocales*, *Sphaeropleales*, and *Chlamydomonadales* orders may play an important role in freshwater ecosystems as primary producers and contribute to algal blooms under certain conditions. The *Chlamydomonadales* order, already present at the base of the core in low abundance, also increased statistically after 2015. Following similar trajectories, diverse orders of the *Ciliophora* taxonomic group demonstrated the same acceleration during the same period (i.e., *Spathidiida*, *Colpodida*, *Peritrichida*, or *Hymenostomatida* were the dominant orders of this group). Previous studies have reported the potential of *Chlorophyta* and *Ciliophora* as a biological marker to track local/global pressures or eutrophication processes (Fig. 7) (*21*, *41*). Other organisms demonstrated the same patterns as those of the *Rhizaria* taxonomic group (i.e., *Eutreptiida*, *Proleptomonas*, *Euglenales*, and *Euglenida*, the two latter demonstrating a sharp increase after 2015). As for the *Chlorophyta* and *Ciliophora*, previous research emphasized that nutrient-rich environments can create favorable conditions for these protists by providing food resources, which may lead to an increase of their abundance. Human activities such as deforestation and agriculture expansion can create favorable conditions for the proliferation of opportunistic species such as *Eutreptiida*, *Proleptomonas*, *Euglenales*, and *Euglenida*, which are often resilient to environmental changes. The greater abundance of these organisms likely further indicates the occurrence of eutrophication processes and the degradation of water quality during the first cyanobacterial bloom reported in this reservoir in 2015 by French authorities. In the absence of high inputs of fertilizers or human-animal fecal matter, the impact of high inputs of soil nutrient during the first erosion period associated with a decrease of the water level during the water crisis (inducing a potential increase of water temperature and a decrease of oxygen) may explain the proliferation of these organisms. In a report commissioned by the French authorities following the 2019–2020 cyanobacterial bloom, the

impact of release and internal recycling of organic matter was highlighted. This recycling likely provides nutrients in a form that can be directly assimilated by Cyanobacteria. Since 2015 and the introduction of regular monitoring of these cyanobacteria (Fig. 4), more than 69 bloom episodes (with concentrations exceeding 100,000 cells/ml) have been observed, including 22 in 2017 and 23 in 2019 (with maximum concentrations of 910,000 and 440,000 cells/ml) (values provided by the company managing the reservoir, i.e., SMAE). Unexpectedly, other protists (member of a group of diverse eukaryotic, predominantly unicellular microscopic organisms) from marine origin were also detected with our *Sed*DNA results, as well as submerged marine macrophytes (*Halodule* taxa). These protists (e.g., *Colpodellida and Ebriida* orders) and plant follow the same trajectory as those described above. This plant was observed in the vicinity of the dam and led to problems for the dam's maintenance. The detection of these marine species can be explained by the proximity of the Dzoumogné reservoir to the sea (i.e., 1800 m away), where humans and animals can mediate the transfer between the two environments (e.g., boats from the sea are often used for maintenance of the dam, animals such as cows can move freely between both environments). The high production of food associated with these algae and microorganism production can explain the increasing abundance of invertebrates and fish communities located on top of the trophic chain.

As an example, *Cyclopoida* (order of freshwater shellfish, only represented by the *Cyclopidae* family in our sequence) followed the same trajectory as the algae and protists described above. This organism plays an important role in nutrient cycling and for controlling algal populations. They also provide a prey for a wide range of organisms, including fish. As a response to the food availability, the fish community also increased during this period. As described by Barouillet *et al.* (*21*), fish communities provide an integrated response of the reservoir to the environmental stressor. Their diversity is not often reported in *Sed*DNA studies. In the Dzoumogné reservoir, two main orders of freshwater fishes were detected (*Cypriniformes* and *Cyprinodontiformes*). Change in aquatic DNA communities after 2016 provides insights into the consequences of climatic and anthropogenic stressors on the destabilization of the aquatic environment.

The multiproxy approach developed in this study demonstrated the unprecedented and rapid consequences of associated anthropogenic and climatic stressors on water and soil resources threatening the fragile and limited natural resources of this island in less than 15 years. The trajectory of this degradation will likely continue to accelerate in the coming years as the population is expected to further increase (migration and high fertility index) by 40 or 145% in Mayotte island by 2050 (according to the best and worst case scenario projections), as expected more widely in the entire Comoros region (whose population is expected to reach 2 million by 2050, an increase of 74% between 2019 and 2050, or 950 persons/km^2) or Madagascar island (+103% between 2022 and 2050, from 29 to 59 million inhabitants), (United Nations, World Population Prospects 2022, https://population.un.org/wpp/). According to the United Nations, in addition to demographic growth, these regions will be challenged by the effects of climate change with alternating periods of prolonged drought and heavy rainfall, with the risk of exacerbating water crises, natural disasters (e.g., muddy floods and landslides), and desertification processes. The Mayotte island has already undergone profound changes since the sample collection with the appearance of mechanization (e.g., use of small tractors for farming) and the increasing use of agricultural inputs (e.g., illegal pesticide and probably fertilizer imports from the neighboring islands). The water quality of the reservoir is also degrading with a recent manganese contamination further increasing the pressure on water resources already observed in this study (e.g., siltation and eutrophication). With the current deforestation rate (1.2% per year), the forest of Mayotte Island is expected to have fully disappeared by 2070, which will cause an irremediable loss of biodiversity. These Comoros islands are an emblematic example of the consequence of deforestation processes in land degradation. There are more than 45,000 islands (>0.5 km^2) within the tropics, mainly in developing countries, regrouping more than 115 million habitants (*42*). These islands are facing, for most of them, the challenges reported in this study (e.g., Sri Lanka and Haiti). Mayotte is a European territory with laws/regulations to protect the environment and the citizens, which makes it different from most of these islands. For example, during the last water crisis in 2023, 17 million liters of bottled water imported from mainland France were distributed monthly. However, this management solution may only be temporary, given the urgency of the environmental crises reported in the current research. For the thousands of tropical islands that could suffer from these erosion and water crises in the coming decades, these emergency measures would be impossible to support and generalize because of their huge cost and their unsustainable character. Managing the situation therefore requires long-term adaptation. The implementation of land conservation measures and the increase in farmer's awareness of the deleterious impacts of ongoing practices will therefore be essential to reduce the risk of occurrence of major socio-environmental crises in the coming years under the projected growth of population, major land use changes, and increasing climatic pressures in these tropical island in particular and this world's region in general.

MATERIALS AND METHODS

Site

Located in the Indian Ocean between Madagascar and the coast of Mozambique, the island of Mayotte (374 km^2) is part of the Comoros archipelago. It is the oldest of these four large volcanic islands (7.7 million years old), the easternmost island of the archipelago (Fig. 1). Geopolitically, Mayotte voted overwhelmingly to remain under French administration in 1974 when Comoros gained independence from France, leading to its status as an overseas department in 2011 and European Union's outermost region in 2014. The island's revised administrative status, coupled with its relative prosperity compared to neighboring regions, has made it an attractive destination for immigrants, mainly from nearby Comoros and other countries (e.g., Madagascar and different African countries). They come in search of better economic opportunities, access to health care, and educational resources. This uncontrolled migratory flow, combined with a high birth rate, has led a to rapid and continuous population growth of +80% in just 20 years (between 2002 and 2021). The French government estimates that in 2021, there were more than 310,000 people living on the island. This does not include illegal immigrants as their number is difficult to estimate. This influx of people has created major challenges for this small territory. It has strained infrastructure, social services, and environmental resources, exacerbated existing socio-economic disparities and sparked debates on immigration policy and integration strategies.

Water availability is one of the main challenges faced by this island. Drinking water is mainly extracted from surface waters, with

40% from rivers and 20% from the two hillside reservoirs (Dzoumogné and Combani) (Figs. 1 and 2). The rest comes from groundwater (32%) and a desalination plant installed in "Petite Terre" (8%) (Fig. 1). Most of the water is used for domestic purposes (85%), about 10% for agriculture, and less than 5% for industrial or recreational purposes. According to the French state, the average water demand in 2050 will amount to between 93,000 and 104,000 m^3/day, and the current production is already insufficient (38,000 m^3/day) to meet the current demand (42,000 m^3/day) (*43*). This growing demand for water, combined with the increased occurrence of periods of drought, has plunged Mayotte Island into severe water crises, which have worsened since 2017. In addition, the increase of population led to an unprecedented land use change mainly driven by deforestation under the joint pressure of agricultural expansion and uncontrolled urbanization leading to landscape fragmentation (on Fig. 1, the picture on the left highlights the processes of hand-made deforestation on the island). This land use change induces a destabilization of the sedimentary cascade, inducing the accelerated siltation of the lagoon, making the island more vulnerable to natural hazards (e.g., muddy floods and landslides) (*11*).

The Dzoumogné reservoir (22 ha, built in 2002, average depth of 8.5 m) located on the northern part of the island is a strategic site for water security of this territory (Figs. 1 and 2). This reservoir drains a 1038-ha catchment nowadays (in 2022) dominated by natural vegetation (55%; mix of forest and shrub formations), intensive cropland (30%; dominated by the monoculture of banana and cassava), and by traditional agriculture (15%; "Mahorais garden"). No human settlement is found in the catchment; housing is concentrated downstream of the reservoir, in the village of "Dzoumogné" (Fig. 2). On the basis of aerial photography analysis, it was possible to draw the main trend of land use change in this catchment (*44*). The proportion of forest has decreased by 5% in 13 years, from 63% of the catchment area in 2008 to 58% in 2021. Agriculture such as banana plantations (+7% in 18 years), cassava (+6% in 18 years), and ylang-ylang plants have been developed as a result of deforestation of small patches. Intensive banana and cassava cultivation represented 15% of the cultivated area in the basin in 2003. By 2021, it will represent more than 50% of the cultivated area. They are cultivated on the whole land, as a patchwork, very often on rather steep slopes of up to 20% and without any soil protection (*44*). Agricultural practices in this catchment are changing rapidly, with a decline in traditional farming practices, the implementation of a complex agroforestry system combining different cultivated and uncultivated species growing at different levels above the ground (*8*). This intensification of agricultural practices while leaving soil bare below the plantations is one of the main challenges of this catchment. The island has a humid tropical climate with strong annual contrasts [1500 mm per year on average (meteofrance.fr)]. The year is characterized by two main seasons, one hot and rainy (November to March), the other cooler and drier (June to October), separated by two shorter inter-seasons. Elevation is ranging between 59 and 451 m a.s.l. in the Dzoumogné catchment. The island of Mayotte has ferralitic soils showing varying degrees of weathering due to its volcanic nature and tropical climate. The Dzoumogné catchment area is dominated by two morpho-pedological units. The main one is described in the French classification as "reworked Ferrisols" (or Nitisols), followed by the Padza formation, which is located on the ridges of the catchment area, mostly on steep slopes, and corresponding to alterites (*45*).

Sampling

Sediment cores ($n = 5$) were collected in the Dzoumogné reservoir in September 2021 using a 63-mm Uwitec gravity corer equipped with a 100-cm polyvinyl chloride (PVC) liner. Sedimentary archives were retrieved in contrasted accumulation areas detected with the sonar (Lawrence HDS7) to characterize the heterogeneity of sediment properties and accumulation rates across the reservoir (Fig. 2). These samples are identified as DZOU-01 [International Generic Sample Number (IGSN) no: 10.58052/IEFOU0001]; DZOU-02 (IGSN no: 10.58052/IEFOU0002); DZOU-03 (IGSN no: 10.58052/IEFOU0003); DZOU-O4 (IGSN no: 10.58052/IEFOU0004); and DZOU-05 (IGSN no: 10.58052/IEFOU0005). During the field survey, the sonar was used to generate a bathymetric map (composed of 5700 measurement points, the corresponding map was generated with QGIS after correction of water level) to compare the bathymetry in 2021 to the morphology observed before the dam impoundment in 1999. This bathymetric map comparison was used for estimating the volume of sediment accumulated in this reservoir (i.e., this information was used for the erosion rate reconstruction).

In addition, representative sediment source samples ($n = 72$) were collected across the catchment drained by the reservoir for comparing the properties of the sediment accumulated in the reservoir with those of potential sources of erosion. To this end, 20 g of the material (≈2 uppermost cm of the soil) was collected using a metallic trowel across areas representative of the different erosional processes (e.g., surface and subsurface erosion) and land uses (e.g., forest and croplands) observed in this catchment. These samples were sieved to 2 mm for the analyses detailed below.

Nondestructive analyses

The Avaatech XRF core scanner available at the Laboratoire des Sciences du Climat et de l'Environnement was used to obtain high resolution (0.1 cm) and semiquantitative (counts per second) values of geochemical element contents along the core. These data were used for characterizing potential changes in sediment sources throughout time. The titanium (Ti) proxy was specifically used for identifying changes in detritical material contributions (fig. S1) (*46*).

Noncalibrated sediment density was recorded every 0.6 mm along the sediment sequences using computed tomography scanner (CT-Scan) images obtained using the equipment (GE Discovery CT750 HD) available at the DOSEO platform (French Atomic Energy and Alternative Energy Commission, CEA Paris-Saclay, France). Relative density values (derived from CT-number) were extracted from the reconstructed scanner images using the free Matlab application Core-CT (*47*). The relative values of dry bulk density (DBD) were calibrated by measuring the absolute DBD (gram per cubic centimeter) in 20 samples collected along the cores (obtaining a r^2 of 0.8, 0.93, 0.91, 0.92, and 0.95 between DBD and CT-number for DZOU-01, 02, 03, 04, and 05 cores, respectively).

Fallout radionuclide analyses were performed by gamma spectrometry on a selection of samples collected on the DZOU-05 core ($n = 26$) and all sediment sources samples ($n = 72$) using coaxial N- and P-type HPGe detectors (Canberra/Ortec) available at the Laboratoire des Sciences du Climat et de l'Environnement (Gif-sur-Yvette, France) for quantifying their activity concentrations in ^{137}Cs (ceasium-137) originated from global fallout associated with bomb testing and the continuous $^{210}Pb_{ex}$ (excess of lead-210) fallout with rainfall (*48*).

Energy-dispersive XRF measurements (Epsilon 3, Malvern Panalytical) were conducted on the same selected samples along the DZOU-05 sediment cores as for the radionuclide analyses and on the potential sediment source samples to obtain concentrations in major elements (i.e., Mg, Al, Si, Ti, K, Ca, Cr, Mn, Fe, Ni, Cu, Zn, As, Rb, Sr, Zr, and Pb) and compare the geochemical signature found in both the sources and sediment accumulated in the reservoir.

Visible colorimetry was measured for soil and sediment samples using a portable diffuse reflectance spectrophotometer Konica Minolta CM-700d, set on a 3-mm target radius. The spectrophotometer was calibrated before measurements using a zero and white standards. Measurements were conducted according to D65 illuminance standard, 10° angle observer and excluding the specular component. The spectral reflectance (in %) was measured each 10 nm within the visible range 360 to 740 nm. CIELAB color space parameters (i.e., L*, a*,b*) were determined.

Destructive analyses

IRMS analyses were conducted on dry sediment for determining organic matter properties, including elemental concentrations (TOC and total nitrogen, TN, both expressed in %) and stable isotope measurements ($\delta^{13}C$ and $\delta^{15}N$, expressed in ‰). These measurements were performed with a continuous flow Elementar VarioPyro cube analyzer coupled to a Micromass Isoprime IRMS available at the Alysés platform of the Institut de Recherche pour le Développement (IRD, Bondy, France) on a selection of 100 samples (respectively, 28 samples for the DZOU-05 core and 72 samples for the potential sources of sediment). Results of these analyses are available on the Zenodo repository at: https://zenodo.org/records/8403071.

Sediment core dating

Age models were established by fitting the meteorological data (rainfall) measured at the M'tsamboro station (≈4 km from the Dzoumogné reservoir) (these data are freely available at: https://doi.pangaea.de/10.1594/PANGAEA.935780) with the terrigenous proxies (Ti) extracted from the XRF core scanner analyses performed for each sediment core. This method was used as an alternative approach in the absence of trend in radionuclides activities (i.e., described in the Results). The hypothesis of this approach is that the climate of Mayotte Island is characterized by an alternation of pronounced dry and humid seasons (typically from December to March), promoting alternatively the accumulation of autochthonous and terrigenous sediment during erosion processes. These alternations were visually observed in the cores and with the XRF analyses demonstrating a high terrigenous content (associated with high Ti content) during humid seasons associated with sediment transported as compared to low values during dry seasons (characterized by low sediment transfer). This type of approach were already used previously (*49*). Correlation ($r^2 = 0.65$) between these temporal and measured series was performed using the updated version of the free software Analyseries (*50*) and Qanalyseries (*51*) (fig. S1). Age model was validated by identifying the contrasted periods of sediment delivery (highs and lows) and by the identification of DNA species characteristic of some events (e.g., detection of green algae species simultaneously to cyanobacteria bloom in 2015, highest erosion rate during the landscape fragmentation period).

Erosion rate reconstruction

The mass accumulation rate (MAR, expressed in gram per square centimeter per year), corresponding to the amount of organic and terrigenous material deposited at each individual coring site was reconstructed by multiplying the high-resolution DBD extracted from the calibrated tomography scanner profiles (expressed in gram per cubic centimeter) with the sediment accumulation rate (SAR, centimeter per year) provided by the age model (Eq. 1) (*52*)

$$\mathrm{MAR}\ (\mathrm{cm}^{-2}\ \mathrm{year}^{-1}) = \mathrm{DBD}\ (\mathrm{g\ cm}^{-3}) \times \mathrm{SAR}\ (\mathrm{cm\ year}^{-1}) \quad (1)$$

The volume of sediment accumulated in the Dzoumogné reservoir was reconstructed by multiplying the MAR of each individual core with the surface of influence around the corresponding cores. This approach appeared to be more accurate to take into account the variability of sediment properties and dynamics within the reservoir (e.g., deltaic areas versus vicinity of the dam can show different sediment properties). Most studies reconstructing erosion propagated the average sediment flux reconstructed from one core to the entire lake or reservoir. In our study, these influence areas were automatically computed with the free software QGIS according to the reservoir morphology (available from the bathymetric data) and the distance between the cores. The representativeness of the cores within these influence areas represents the main source of uncertainty in the reconstruction of erosion.

To assess the representativeness of each core within these areas, we have compared the thickness of sediment at each coring site with the average sediment thickness (and SD) within the influence area (sediment thickness was estimated by comparing the initial and last bathymetric survey, in 1999 and 2021, respectively). These comparisons demonstrated that sediment thickness is not homogenous within these areas. On average, SRs are 40 to 63% higher at the coring site than within the influence area according to the core location. (For example, the SR was 40% higher at the DZOU-05 coring site than across the influence area around the core). This overestimation was taken into account for each core to obtain the MARcor (corrected Mass Accumulation Rate). The MARcor corresponds to the average sediment flux across the influence area. (SD from sediment thickness was used for estimating the error of volume estimation per influence area. This error was propagated to estimate the error of soil erosion.)

To obtain the corresponding volume accumulated for each area (VS, expressed in tonne per year), the influence surfaces (IS, expressed in hectare) were multiplied with the MARcor (gram per square centimeter per year was converted into tonne per hectare per year) (Eq. 2). Then, the volume of each influence area (e.g., VS1, VS2, VS3…) were summed to obtain the total volume of sediment accumulated in the reservoir throughout time (VR, expressed in tonne per year) (Eq. 3)

$$\begin{aligned}&\mathrm{VS\ (tonne\ per\ year)} = \\ &\mathrm{MARcor\ (tonne\ per\ hectare\ per\ year)} \times \mathrm{IS\ (hecatre)}\end{aligned} \quad (2)$$

$$\begin{aligned}&\mathrm{VR\ (tonne\ per\ year)} = \mathrm{VS1\ (tonne\ per\ year)} + \\ &\mathrm{VS2\ (tonne\ per\ year)} + \mathrm{VS3\ (tonne\ per\ year)} + \\ &\mathrm{VS4\ (tonne\ per\ year)} + \mathrm{VS5\ (tonne\ per\ year)}\end{aligned} \quad (3)$$

The erosion rate (ER, expressed in megagram per hectare per year) was calculated by dividing the volume of sediment accumulated over time by the catchment surface area (CS, expressed in hectare) (Eq. 4). The catchment surface was artificially increased from 724 to 1038 ha after 2017. This increase occurred after an operation of

landscape management that connected an additional sub-catchment to the Dzoumogné reservoir

$$\text{ER (megagram per hectare per year)} = \text{CS (hectare)} \times \text{VR (tonne per year)} \quad (4)$$

Sediment fingerprinting and mixing model

Sediment fingerprinting involves the analysis of biophysicochemical characteristics of sediment to identify their sources and pathways across a catchment. By identifying and quantifying these signatures, such as those provided by geochemistry, organic matter content, and color properties, it is possible to trace sediment accumulated in the reservoir back to their specific land use/geology/soil type origin or geomorphological processes (*53*). To quantify the contribution of sediment sources to material accumulated in the Dzoumogné reservoir, sediment fingerprinting was applied to the DZOU05 sediment core. The application of the sediment fingerprinting approach is based on a three-step method (*54*). The first step is to assess the conservativeness of the tracers. Tracer conservativeness in sediment fingerprinting ensures that selected tracers remain unchanged during sediment transport. This allows an accurate attribution of sediments to their original sources. The second step consists of evaluating the discriminating power of potential tracers. In this step, the potential of the tracers to effectively discriminate between sediment sources on the basis of measured properties is evaluated. The last step is a forward stepwise selection for the identification of the best subset of tracers. Conservativeness evaluation consists of selecting properties for which target (i.e., sediment core sections) values are all included in the range of the sources (i.e., cropland, forest, and subsoil). To this end, range tests based on mean and median values of source groups were applied using the range.tests function from FingR package (*54*).

The capacity of properties to discriminate among sources was assessed using a two-samples Kolmogorov-Smirnov test. This test compares the location and shape of the distribution of the two samples. It was applied for each pair of source groups. A property is considered as discriminant when at least one of the source pairs is statistically different (i.e., P value <0.05).

To identify a subset of tracers among the selected ones that maximize the differences between groups, a forward stepwise variable selection was performed using the greedy.wilks function from the klaR package. Thus, the tracer selection procedure resulted in the selection of: one radionuclide (^{137}Cs), one organic matter property (TOC), three geochemical properties (Al, Ca, and Sr), and two colorimetric parameters (L*, a*). Figure S2 shows the evolution of sediment properties over time in comparison to the properties of the selected tracers. The set of selected tracers was used in an unmixing model to quantify the source contributions in the sediment core DZOU-05 between three main sources: forest, cropland, and subsoil. The subsoil source corresponds to channel bank erosion (across the catchment or along the reservoir borders), along with sediment supply from unpaved road, badland, and gully erosion sources. A stochastic model based on Bayesian structure, i.e., the Mean model (*55*), was run to obtain the sediment sources contribution for each layer of the sediment core.

*Sed*DNA extraction

DNA was extracted from 12 samples collected along the DZOU-03 core 3 weeks after the core collection. From the collection of this sedimentary archive to the extraction of the DNA samples, the sediment core was stored in a dark and cold room (4°C). The sediment core was opened and sampled under a controlled environment to limit the contamination risk following the recommendations of previous publications (*13*, *56*). The core was precut on a cutting bench before being placed in a fume cupboard in a biological clean room. The fume cupboard had previously been cleaned with DNA cleaner and ultraviolet. The core was divided into two parts using sterilized PVC plates by operators wearing gowns, gloves, masks, and headgear. To extract each sample from the core, sterilized metal plates were inserted on either side. The central part of this sample was then subsampled to remove the part of the sediment contacting the PVC tube of the core and the cutting tools. A blank was placed in the fume cupboard to control contamination during core opening and sampling.

*Sed*DNA was retrieved using a standardized protocol that combines the use of commercial kits (Nucleospin soil, Macherey-Nagel) and the extracellular DNA pretreatment described in Taberlet *et al.* (*57*). To limit amplification biases and to improve the metabarcoding sensitivity, a combination of seven genetic markers was used to polymerase chain reaction (PCR) amplify each targeted taxonomic group [plants, 50 to 70 bp, trnL (*58*); plants, 150 bp, rbcL (*59*); plants/fungi, 320 bp, ITS (*60*); plants, 380 bp, ITS; metazoa, 200 bp, 16*S* (*61*); eukaryotes, 200 bp, 18S (*62*); vertebrates, 200 bp, 12*S* (*63*)]. PCRs were realized in octuplicates with positive and negative controls. Extraction controls were also amplified with the dedicated primers. PCR products were cleaned using the MinElute purification kit (QIAGEN), and all purified amplicons were pooled in equimolar concentrations at the exception of the extraction and the PCR negative controls as they were not concentrated enough. Then, each sample pool was run on an Agilent Bioanalyzer using the DNA High Sensitivity LabChip kit (Agilent Technologies, Santa Clara, CA, USA) to verify amplicon length, and each sample was finally quantified with a Qubit fluorometer (Invitrogen, Carlsbad, CA, USA).

Libraries were generated with a PCR-free protocol to tremendously reduce the number of chimeras induced by the metabarcoding approach. One microgram of each purified PCR products pool was submitted to molecular end-repair and then ligated to Illumina adapters before sequencing on Illumina platforms (Next-Generation Sequencing; Fasteris, Switzerland) using a NovaSeq instrument (Illumina, San Diego, CA, USA) with a paired-end read mode covering the amplicon lengths. The objective was to obtain approximately 1 million reads per marker and per sample.

Bioinformatics analyses were performed using the OBITools (*64*) and QIIME2 (*65*) pipelines. Reads were first demultiplexed using OBITOOLS. Then, erroneous sequences were removed, and singletons were filtered out. Sequences were then clustered at 97% identity using VSEARCH (*66*). Sequences that were found in the extraction blanks were removed from the downstream analysis. Taxonomic assignment was realized in two steps. First, sequences were assigned by blasting them against a custom database generated from the GenBank latest release curated and restricted to all the documented taxa. Sequences with more than 95% identity match were kept, and their last common ancestor was computed using MEGAN (*67*). A second assignment pass was made using a Naïve Bayesian Classifier using QIIME's rescript plugin (*68*).

To study the possible impact of sequence degradation on the reads obtained, a linear model (Eq. 5) was performed to assess the impact of sequence lengths on the number of reads obtained (table S3). The underlying idea was that if degradation occurred, longer reads would be negatively and significantly affected in the different samples, more particularly in deeper samples. The extraction method was also considered

in the model to account for the potential impact of the extraction method on the number of reads sequenced. The model was applied on rarefied reads to remove the potential biases induced by library pooling

$$\log_{10}(\text{number of reads}) \sim \text{seq. length}^{*}\ \text{depth} + \text{extraction method} \quad (5)$$

Statistical and data analysis

Data analysis was performed by following the recommendations of Chen and Ficelota and Picard *et al.* (*29*, *69*). To identify significant shifts in multivariate data, we used a combination of dimensionality reduction techniques and clustering algorithms. First, we used PCA to reduce the dimensionality of our dataset while preserving its variability. Successive observations were then connected in ordination space, allowing us to identify major shifts in community composition. In addition, we plotted the scores of principal components over time to detect change points. To further refine our analysis, we applied incremental sum of squares (CONISS) clustering methods to identify the timing of community changes.

RDA and CCA were performed to assess the correlation between environmental variables (e.g., erosion rate, meteorological parameters, and sediment sources) and taxonomic composition. Permutation tests were conducted to evaluate the statistical significance of these relationships. A P value <0.05 was used for these tests.

Univariate AMOC was used for identifying breaking points or significant shifts in data series. This method examines the mean value of the counts within sliding windows along the data series. When a significant deviation is detected in the mean count within a window compared to the overall mean, it indicates a potential breaking point or shift in the data series.

To compute diversity metrics, reads were first rarefied with replacement using QIIME2. Because of the disparity in recovered sequence sequencing depth, some samples had to be filtered out from this rarefaction step. This was particularly the case with the extracellular DNA treatment that yielded lower reads and OTUs. As a consequence, samples extracted using this method were removed from diversity metrics computations. Various diversity metrics were then computed using the diversity plugin available in QIIME2. Last, two-way crossed analysis of variance (ANOVA) was performed to determine the impact of temporal categories on the diversity metrics while controlling for the extraction buffer used. These biodiversity metrics are provided in the Supplementary Materials (table S1). A P value <0.05 was used for these tests. Statistical analyses were performed in R (version 4.2.3).

Supplementary Materials

This PDF file includes:

Supplementary Text
Figs. S1 to S8
Tables S1 to S3

REFERENCES AND NOTES

1. United Nations Department of Economic and Social Affairs, World Population Prospects 2022: Summary of Results (2022); https://www.un.org/development/desa/pd/sites/www.un.org.development.desa.pd/files/wpp2022_summary_of_results.pdf.
2. T. M. Lenton, C. Xu, J. F. Abrams, A. Ghadiali, S. Loriani, B. Sakschewski, C. Zimm, K. L. Ebi, R. R. Dunn, J.-C. Svenning, M. Scheffer, Quantifying the human cost of global warming. *Nat. Sustain.* **6**, 1237–1247 (2023).
3. M. McAuliffe, A. Triandafyllidou, World Migration Report 2022 (2021).
4. F. Zabel, R. Delzeit, J. M. Schneider, R. Seppelt, W. Mauser, T. Václavík, Global impacts of future cropland expansion and intensification on agricultural markets and biodiversity. *Nat. Commun.* **10**, 2844 (2019).
5. M. M. Maja, S. F. Ayano, The impact of population growth on natural resources and farmers' capacity to adapt to climate change in low-income countries. *Earth Syst. Environ.* **5**, 271–283 (2021).
6. A. Foucher, M. Tassano, P.-A. Chaboche, G. Chalar, M. Cabrera, J. Gonzalez, P. Cabral, A.-C. Simon, M. Agelou, R. Ramon, T. Tiecher, O. Evrard, Inexorable land degradation due to agriculture expansion in South American Pampa. *Nat. Sustain.* **6**, 662–670 (2023).
7. C. Guerrero-Pineda, G. D. Iacona, L. Mair, F. Hawkins, J. Siikamäki, D. Miller, L. R. Gerber, An investment strategy to address biodiversity loss from agricultural expansion. *Nat. Sustain.* **5**, 610–618 (2022).
8. J. Huat, M. Nagy, A. Carpente, M. Schwartz, T. Le Bourgeois, P. Marnotte, Guide de la flore spontanée des agrosystèmes de Mayotte (2021).
9. J. Zinke, J. J. G. Reijmer, B. A. Thomassin, W.-C. Dullo, P. M. Grootes, H. Erlenkeuser, Postglacial flooding history of Mayotte Lagoon (Comoro Archipelago, southwest Indian Ocean). *Mar. Geol.* **194**, 181–196 (2003).
10. S. B. Tebbett, C. H. R. Goatley, D. R. Bellwood, Fine sediments suppress detritivory on coral reefs. *Mar. Pollut. Bull.* **114**, 934–940 (2017).
11. V. Landemaine, J.-F. Desprats, G. Dectot, B. Vignerot, O. Cerdan, J.-D. Rinaudo, E. Carme, K. Said, M. Vitter, S. Salvador-Blanes, P. Vanhooydonck, A. Mavouna, Suivi hydro-sédimentaire et modélisation de l'érosion des sols à Mayotte–Projet LESELAM 2, (Orléans, France, 2021); http://ficheinfoterre.brgm.fr/document/RP-70572-FR.
12. K. Wolka, J. Mulder, B. Biazin, Effects of soil and water conservation techniques on crop yield, runoff and soil loss in sub-Saharan Africa: A review. *Agric. Water Manag.* **207**, 67–79 (2018).
13. E. Capo, C. Giguet-Covex, A. Rouillard, K. Nota, P. D. Heintzman, A. Vuillemin, D. Ariztegui, F. Arnaud, S. Belle, S. Bertilsson, C. Bigler, R. Bindler, A. G. Brown, C. L. Clarke, S. E. Crump, D. Debroas, G. Englund, G. F. Ficetola, R. E. Garner, J. Gauthier, I. Gregory-Eaves, L. Heinecke, U. Herzschuh, A. Ibrahim, V. Kisand, K. H. Kjær, Y. Lammers, J. Littlefair, E. Messager, M.-E. Monchamp, F. Olajos, W. Orsi, M. W. Pedersen, D. P. Rijal, J. Rydberg, T. Spanbauer, K. R. Stoof-Leichsenring, P. Taberlet, L. Talas, C. Thomas, D. A. Walsh, Y. Wang, E. Willerslev, A. van Woerkom, H. H. Zimmermann, M. J. L. Coolen, L. S. Epp, I. Domaizon, I. G. Alsos, L. Parducci, Lake sedimentary DNA research on past terrestrial and aquatic biodiversity: Overview and recommendations. *Quaternary* **4**, 6 (2021).
14. J. A. Dearing, R. T. Jones, Coupling temporal and spatial dimensions of global sediment flux through lake and marine sediment records. *Glob. Planet. Change* **39**, 147–168 (2003).
15. A. C. Gellis, R. M. T. Webb, S. C. McIntyre, W. J. Wolfe, Land-use effects on erosion, sediment yields, and reservoir sedimentation: A case study in the Lago Loíza Basin, Puerto Rico. *Phys. Geogr.* **27**, 39–69 (2006).
16. J. Von Eggers, M.-E. Monchamp, E. Capo, C. Giguet-Covex, T. Spanbauer, P. D. Heintzman, Inventory of ancient environmental DNA from sedimentary archives: Locations, methods, and target taxa. Zenodo (2022); 10.5281/ZENODO.6847522.
17. R. Dommain, M. Andama, M. M. McDonough, N. A. Prado, T. Goldhammer, R. Potts, J. E. Maldonado, J. B. Nkurunungi, M. G. Campana, The challenges of reconstructing tropical biodiversity with sedimentary ancient DNA: A 2200-year-long metagenomic record from Bwindi impenetrable forest, Uganda. *Front. Ecol. Evol.* **8**, 218 (2020).
18. C. Giguet-Covex, J. Pansu, F. Arnaud, P.-J. Rey, C. Griggo, L. Gielly, I. Domaizon, E. Coissac, F. David, P. Choler, J. Poulenard, P. Taberlet, Long livestock farming history and human landscape shaping revealed by lake sediment DNA. *Nat. Commun.* **5**, 3211 (2014).
19. L. Parducci, K. D. Bennett, G. F. Ficetola, I. G. Alsos, Y. Suyama, J. R. Wood, M. W. Pedersen, Ancient plant DNA in lake sediments. *New Phytol.* **214**, 924–942 (2017).
20. I. G. Alsos, P. Sjögren, M. E. Edwards, J. Y. Landvik, L. Gielly, M. Forwick, E. Coissac, A. G. Brown, L. V. Jakobsen, M. K. Føreid, M. W. Pedersen, Sedimentary ancient DNA from Lake Skartjørna, Svalbard: Assessing the resilience of arctic flora to Holocene climate change. *Holocene* **26**, 627–642 (2016).
21. C. Barouillet, M. Monchamp, S. Bertilsson, K. Brasell, I. Domaizon, L. S. Epp, A. Ibrahim, H. Mejbel, E. C. Nwosu, J. K. Pearman, M. Picard, G. Thomson-Laing, N. Tsugeki, J. Von Eggers, I. Gregory-Eaves, F. Pick, S. A. Wood, E. Capo, Investigating the effects of anthropogenic stressors on lake biota using sedimentary DNA. *Freshw. Biol.* **68**, 1799–1817 (2023).
22. L. S. Epp, K. R. Stoof, M. H. Trauth, R. Tiedemann, Historical genetics on a sediment core from a Kenyan lake: Intraspecific genotype turnover in a tropical rotifer is related to past environmental changes. *J. Paleolimnol.* **43**, 939–954 (2010).
23. J. Krueger, V. Foerster, M. H. Trauth, M. Hofreiter, R. Tiedemann, Exploring the past biosphere of chew Bahir/Southern Ethiopia: Cross-species hybridization capture of ancient sedimentary DNA from a deep drill core. *Front. Earth Sci.* **9**, 683010 (2021).
24. K. M. Ruppert, R. J. Kline, M. S. Rahman, Past, present, and future perspectives of environmental DNA (eDNA) metabarcoding: A systematic review in methods, monitoring, and applications of global eDNA. *Glob. Ecol. Conserv.* **17**, e00547 (2019).
25. L. Bremond, C. Favier, G. F. Ficetola, M. G. Tossou, A. Akouégninou, L. Gielly, C. Giguet-Covex, R. Oslisly, U. Salzmann, Five thousand years of tropical lake sediment DNA records from Benin. *Quat. Sci. Rev.* **170**, 203–211 (2017).

26. P. Taberlet, A. Bonin, L. Zinger, E. Coissac, Environmental DNA: For biodiversity research and monitoring (2018).
27. F. Echeverría-Beirute, I. Varela-Benavides, J. P. Jiménez-Madrigal, M. Carvajal-Chacon, T. Guzmán-Hernández, eDNA extraction protocol for metagenomic studies in tropical soils. *Biotechniques* **71**, 580–586 (2021).
28. S. Boessenkool, G. Mcglynn, L. S. Epp, D. Taylor, M. Pimentel, A. Gizaw, S. Nemomissa, C. Brochmann, M. Popp, Use of ancient sedimentary DNA as a novel conservation tool for high-altitude tropical biodiversity. *Conserv. Biol.* **28**, 446–455 (2014).
29. W. Chen, G. F. Ficetola, Numerical methods for sedimentary-ancient-DNA-based study on past biodiversity and ecosystem functioning. *Environ. DNA* **2**, 115–129 (2020).
30. L. Ferrante, P. M. Fearnside, The Amazon's road to deforestation. *Science* **369**, 634 (2020).
31. N. Labrière, B. Locatelli, Y. Laumonier, V. Freycon, M. Bernoux, Soil erosion in the humid tropics: A systematic quantitative review. *Agric. Ecosyst. Environ.* **203**, 127–139 (2015).
32. V. Sellier, O. Navratil, J. P. Laceby, M. Allenbach, I. Lefèvre, O. Evrard, Reconstructing the impact of nickel mining activities on sediment supply to the rivers and the lagoon of South Pacific Islands: Lessons learnt from the Thio early mining site (New Caledonia). *Geomorphology* **372**, 107459 (2021).
33. T. Grangeon, O. Cerdan, V. Landemaine, R. Vandromme, J. F. Desprats, S. Salvador-Blanes, P. Vanhooydonck, A. Gaillot, L. Maniere, I. Pene-Galland, O. Evrard, A. Foucher, L. Ledieu, A. Simonneau, J. F. Ouvry, L. T. Pak, Les observatoires du ruissellement : Comprendre les processus pour améliorer les modélisations. *La Houille Blanche* **106**, 7–16 (2021).
34. P. Borrelli, D. A. Robinson, L. R. Fleischer, E. Lugato, C. Ballabio, C. Alewell, K. Meusburger, S. Modugno, B. Schütt, V. Ferro, V. Bagarello, K. Van Oost, L. Montanarella, P. Panagos, An assessment of the global impact of 21st century land use change on soil erosion. *Nat. Commun.* **8**, 2013 (2017).
35. O. H. Ralison, A. V. Borges, F. Dehairs, J. J. Middelburg, S. Bouillon, Carbon biogeochemistry of the Betsiboka estuary (north-western Madagascar). *Org. Geochem.* **39**, 1649–1658 (2008).
36. P. Randrianarijaona, The erosion of Madagascar, in *Ambio* (Springer, 1983), pp. 308–311.
37. M. A. Morlock, S. Rodriguez-Martinez, D. Y. Huang, J. Klaminder, Erosion regime controls sediment environmental DNA-based community reconstruction. *Environ. DNA* **5**, 1393–1404 (2023).
38. A. L. Lamb, G. P. Wilson, M. J. Leng, A review of coastal palaeoclimate and relative sea-level reconstructions using $\delta^{13}C$ and C/N ratios in organic material. *Earth Sci. Rev.* **75**, 29–57 (2006).
39. L. Talas, N. Stivrins, S. Veski, L. Tedersoo, V. Kisand, Sedimentary Ancient DNA (sedaDNA) reveals fungal diversity and environmental drivers of community changes throughout the holocene in the present Boreal Lake Lielais Svētiņu (Eastern Latvia). *Microorganisms* **9**, 719 (2021).
40. M. Subiros, E. Brottet, J. L. Solet, A. Leguen, L. Filleul, Health monitoring during water scarcity in Mayotte, France, 2017. *BMC Public Health* **19**, 288 (2019).
41. E. Capo, D. Debroas, F. Arnaud, T. Guillemot, V. Bichet, L. Millet, E. Gauthier, C. Massa, A.-L. Develle, C. Pignol, F. Lejzerowicz, I. Domaizon, Long-term dynamics in microbial eukaryotes communities: A palaeolimnological view based on sedimentary DNA. *Mol. Ecol.* **25**, 5925–5943 (2016).
42. T. N. Browning, D. E. Sawyer, Erosion and deposition vulnerability of small (<5,000 km2) tropical islands. *PLOS ONE* **16**, e0253080 (2021).
43. J. Desprats, V. Landemaine, G. Rolland, C. Colliaux, A. Foucher, S. Lanini, O. Evrard, J. Rinaudo, B. Vignerot, F. Beudard, C. Mucig, O. Cerdan, K. Said, M. Vitter, M. Beltramo, E. Guilloux, M. Arnaud, A. Mavouna, Projet LESELAM 3 (Lutte contre l'Erosion des Sols et l'Envasement du LAgon à Mayotte) - Rapport d'avancement (2021).
44. J. Desprats, J. Lopez, C. Dejan, K. Said, D. Libon, B. Bernard, H. Lousteau, J. Rinaudo, B. Colas, V. Landemaine, Projet LESELAM (Lutte contre l'Erosion des Sols et l'Envasement du LAgon à Mayotte) (2016).
45. E. Latrille, Projet d'inventaire des terres cultivables de Mayotte. Mayotte : Carte morphopédologique et des propositions d'affectation des terres (Montpellier, France, 1981); https://doi.org/10.18167/agritrop/00211.
46. I. W. Croudace, R. G. Rothwell, Micro-XRF studies of sediment cores in *Developments in Paleoenvironmental Research* (Springer, 2015), vol. 17; http://link.springer.com/10.1007/978-94-017-9849-5.
47. Y. T. Yan, S. Chua, T. M. DeCarlo, P. Kempf, K. M. Morgan, A. D. Switzer, Core-CT: A MATLAB application for the quantitative analysis of sediment and coral cores from x-ray computed tomography (CT). *Comput. Geosci.* **156**, 104871 (2021).
48. A. Foucher, P. Chaboche, P. Sabatier, O. Evrard, A worldwide meta-analysis (1977–2020) of sediment core dating using fallout radionuclides including ^{137}Cs and $^{210}Pb_{xs}$. *Earth Syst. Sci. Data* **13**, 4951–4966 (2021).
49. A. Foucher, S. Morera, M. Sanchez, J. Orrillo, O. Evrard, El Niño–Southern Oscillation (ENSO)-driven hypersedimentation in the Poechos Reservoir, northern Peru. *Hydrol. Earth Syst. Sci.* **27**, 3191–3204 (2023).
50. D. Paillard, L. Labeyrie, P. Yiou, Macintosh Program performs time-series analysis. *Eos. Trans. AGU.* **77**, 379–379 (1996).
51. S. Kotov, H. Paelike, QAnalySeries–a cross-platform time series tuning and analysis tool (AGU, 2018); https://agu.confex.com/agu/fm18/meetingapp.cgi/Paper/349843.
52. A. Foucher, O. Evrard, O. Cerdan, C. Chabert, I. Lefèvre, R. Vandromme, S. Salvador-Blanes, Deciphering human and climatic controls on soil erosion in intensively cultivated landscapes after 1950 (Loire Valley, France). *Anthropocene* **34**, 100287 (2021).
53. O. Evrard, P. V. G. Batista, J. Company, A. Dabrin, A. Foucher, A. Frankl, J. García-Comendador, A. Huguet, N. Lake, I. Lizaga, N. Martínez-Carreras, O. Navratil, C. Pignol, V. Sellier, Improving the design and implementation of sediment fingerprinting studies: Summary and outcomes of the TRACING 2021 Scientific School. *J. Soil. Sediment.* **22**, 1648–1661 (2022).
54. T. Chalaux-Clergue, R. Bizeul, P. V. G. Batista, N. Martínez-Carreras, J. P. Laceby, O. Evrard, Sensitivity of source sediment fingerprinting to tracer selection methods. *SOIL* **10**, 109–138 (2024).
55. J. P. Laceby, J. Olley, An examination of geochemical modelling approaches to tracing sediment sources incorporating distribution mixing and elemental correlations. *Hydrol. Process.* **29**, 1669–1685 (2015).
56. L. Parducci, K. D. Bennett, G. F. Ficetola, I. G. Alsos, Y. Suyama, J. R. Wood, M. W. Pedersen, Ancient plant DNA in lake sediments. *New Phytol.* **214**, 924–942 (2017).
57. P. Taberlet, S. M. Prud'Homme, E. Campione, J. Roy, C. Miquel, W. Shehzad, L. Gielly, D. Rioux, P. Choler, J. C. Clément, C. Melodelima, F. Pompanon, E. Coissac, Soil sampling and isolation of extracellular DNA from large amount of starting material suitable for metabarcoding studies. *Mol. Ecol.* **21**, 1816–1820 (2012).
58. P. Taberlet, E. Coissac, M. Hajibabaei, L. H. Rieseberg, Environmental DNA. *Mol. Ecol.* **21**, 1789–1793 (2012).
59. S. W. J. Prosser, P. D. N. Hebert, Rapid identification of the botanical and entomological sources of honey using DNA metabarcoding. *Food Chem.* **214**, 183–191 (2017).
60. T. J. White, T. J. White, T. Bruns, S. Lee, J. Taylor, *Amplification and Direct Sequencing of Fungal Ribosomal RNA Genes for Phylogenetics* (Academic Press, 1990).
61. R. P. Kelly, Making environmental DNA count. *Mol. Ecol. Resour.* **16**, 10–12 (2016).
62. C. M. Hardy, E. S. Krull, D. M. Hartley, R. L. Oliver, Carbon source accounting for fish using combined DNA and stable isotope analyses in a regulated lowland river weir pool. *Mol. Ecol.* **19**, 197–212 (2010).
63. B. Balitzki-Korte, K. Anslinger, C. Bartsch, B. Rolf, Species identification by means of pyrosequencing the mitochondrial 12S rRNA gene. *Int. J. Leg. Med.* **119**, 291–294 (2005).
64. F. Boyer, C. Mercier, A. Bonin, Y. Le Bras, P. Taberlet, E. Coissac, obitools: A unix-inspired software package for DNA metabarcoding. *Mol. Ecol. Resour.* **16**, 176–182 (2016).
65. E. Bolyen, J. R. Rideout, M. R. Dillon, N. A. Bokulich, C. C. Abnet, G. A. Al-Ghalith, H. Alexander, E. J. Alm, M. Arumugam, F. Asnicar, Y. Bai, J. E. Bisanz, K. Bittinger, A. Brejnrod, C. J. Brislawn, C. T. Brown, B. J. Callahan, A. M. Caraballo-Rodríguez, J. Chase, E. K. Cope, R. Da Silva, C. Diener, P. C. Dorrestein, G. M. Douglas, D. M. Durall, C. Duvallet, C. F. Edwardson, M. Ernst, M. Estaki, J. Fouquier, J. M. Gauglitz, S. M. Gibbons, D. L. Gibson, A. Gonzalez, K. Gorlick, J. Guo, B. Hillmann, S. Holmes, H. Holste, C. Huttenhower, G. A. Huttley, S. Janssen, A. K. Jarmusch, L. Jiang, B. D. Kaehler, K. B. Kang, C. R. Keefe, P. Keim, S. T. Kelley, D. Knights, I. Koester, T. Kosciolek, J. Kreps, M. G. I. Langille, J. Lee, R. Ley, Y.-X. Liu, E. Loftfield, C. Lozupone, M. Maher, C. Marotz, B. D. Martin, D. McDonald, L. J. McIver, A. V. Melnik, J. L. Metcalf, S. C. Morgan, J. T. Morton, A. T. Naimey, J. A. Navas-Molina, L. F. Nothias, S. B. Orchanian, T. Pearson, S. L. Peoples, D. Petras, M. L. Preuss, E. Pruesse, L. B. Rasmussen, A. Rivers, M. S. Robeson, P. Rosenthal, N. Segata, M. Shaffer, A. Shiffer, R. Sinha, S. J. Song, J. R. Spear, A. D. Swafford, L. R. Thompson, P. J. Torres, P. Trinh, A. Tripathi, P. J. Turnbaugh, S. Ul-Hasan, J. J. J. van der Hooft, F. Vargas, Y. Vázquez-Baeza, E. Vogtmann, M. von Hippel, W. Walters, Y. Wan, M. Wang, J. Warren, K. C. Weber, C. H. D. Williamson, A. D. Willis, Z. Z. Xu, J. R. Zaneveld, Y. Zhang, Q. Zhu, R. Knight, J. G. Caporaso, Reproducible, interactive, scalable and extensible microbiome data science using QIIME 2. *Nat. Biotechnol.* **37**, 852–857 (2019).
66. T. Rognes, T. Flouri, B. Nichols, C. Quince, F. Mahé, VSEARCH: A versatile open source tool for metagenomics. *PeerJ* **4**, e2584 (2016).
67. D. H. Huson, A. F. Auch, J. Qi, S. C. Schuster, MEGAN analysis of metagenomic data. *Genome Res.* **17**, 377–386 (2007).
68. M. S. Robeson, D. R. O'Rourke, B. D. Kaehler, M. Ziemski, M. R. Dillon, J. T. Foster, N. A. Bokulich, RESCRIPt: Reproducible sequence taxonomy reference database management. *PLoS Comput. Biol.* **17**, e1009581 (2021).
69. M. Picard, J. Von Eggers, K. A. Brasell, D. Yan, J. Klaminder, I. G. Alsos, C. Barouillet, Y. Cheng, R. Dommain, K. Dulias, L. Duxbury, M. E. Edwards, S. G. Pastor, D. Harning, S. M. Hudson, G. Huston, S. Kaynar, L. Kurte, M. Leunda, M. L. D. Lopez, B. Moguel, F. Olajos, V. Pérez, A. Revéret, D. P. Rijal, J. Rydberg, C. Schwörer, K. R. Stoof-Leichsenring, Z. E. Taranu, G. Thomson-Laing, A. Thorpe, R. Tiedemann, L. V. Nogales, Y. Wang, S. A. Wood, E. Capo, Using DNA archived in lake sediments to reconstruct past ecosystems, in *Reference Module in Earth Systems and Environmental Sciences* (Elsevier, 2024); https://linkinghub.elsevier.com/retrieve/pii/B9780323999311001719.

Acknowledgments: This work was part of the LESELAM 3 project. We are grateful to the DOSEO platform (Université Paris-Saclay, CEA, List) and especially to A.-C. Simon and

M. Agelou for performing the tomography scanner measurements on the sediment core sections. We would also like to thank F. Pitois, A. Souffou, and F. Fournial for sharing data on cyanobacteria in the Dzoumogné reservoir. **Funding:** This work was financially supported by the European Agricultural Fund for Rural Development (EAFRD PDR 2014-2022 Mayotte), Centre National de la Recherche Scientifique (CNRS): ANR PIA (ANR-20-IDEES-0002), and Centre National de la Recherche Scientifique (CNRS): AAP INSU EC2CO 2023 (HISTORIFEUX).
Author contributions: Sample collection: A.F., O.E., and O.C. Sediment analyses: L.R. and A.F. Sediment tracing approach: O.E., L.R., R.B., T.C.-C., and A.F. *Seda*DNA analyses: J.M., N.D., and V.A. Writing—original draft: A.F., O.E., O.C., V.L., and J.-F.D. **Competing interests:** V.A. and J.M. are research scientists in a private company that specializes on the use of environmental DNA for species detection. **Data and materials availability:** Data are available in the Zenodo repository at https://zenodo.org/records/8403071 for the results of source and sediment properties and at https://zenodo.org/records/11060223 for the DNA results. All data needed to evaluate the conclusions in the paper are present in the paper and/or the Supplementary Materials.

Submitted 20 December 2023
Accepted 9 July 2024
Published 14 August 2024
10.1126/sciadv.adn5941